Illustrations by F. Cairo

The strange quark as a probe for New Physics in the Higgs Sector

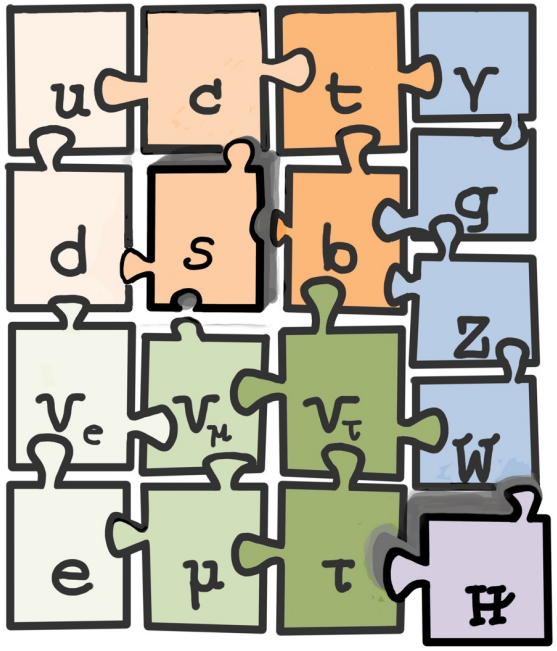

ICHEP 2022 BOLOGNA

ICHEP 2022 XLI
International Conference on High Energy Physics
Bologna (Italy)

6 13 07 2022

Valentina Maria Martina Cairo, **on behalf of the ILD concept group**

CERN

The Post Higgs boson era

2012 → **Now** → **Future**

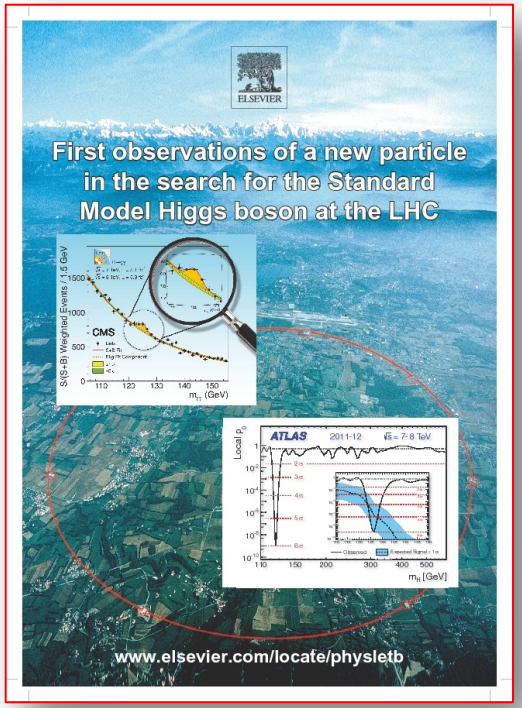

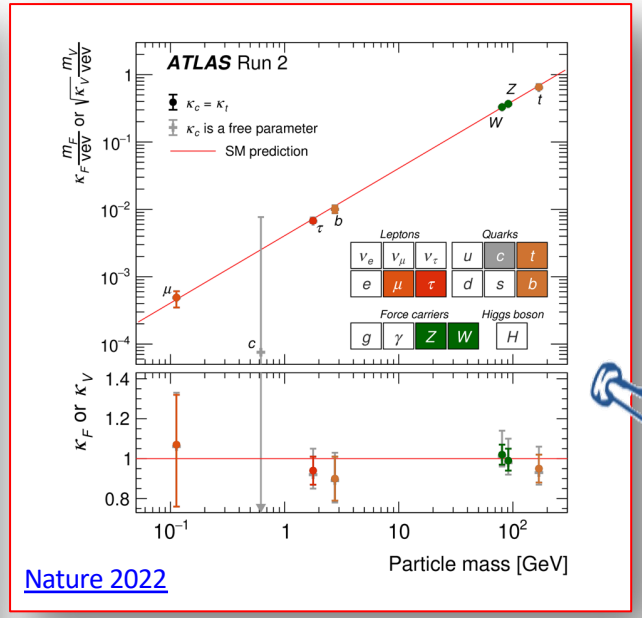

Nature 2022

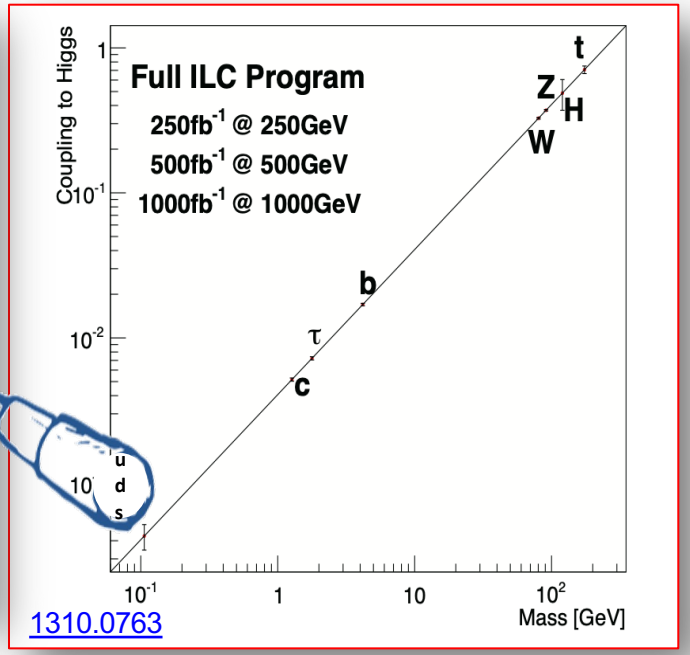

1310.0763

A Higgs boson-like particle was found!

So far, the SM rules, but the exploration has just begun…

Is **Yukawa coupling really universal** between families?

Future Colliders

Symmetry

Illustration by Sandbox Studio, Chicago

Higgs and Flavors in the far future

- Higgs to **top-quarks**
  - No big gain from HL-LHC to e+e- machines (low $\sqrt{s}$)
- Higgs to **b-quarks**
  - ~ 2% at HL-LHC
  - ~ 0.5-1% in future e^+e^- machines
    - x2–4 better than HL-LHC
- Higgs to **c-quarks**
  - HL-LHC able to probe the SM?
  - ~1% in future e^+e^- machines
- Higgs to **light-quarks**
  - Only upper bounds

The Strange Yukawa coupling at e^+e^- colliders

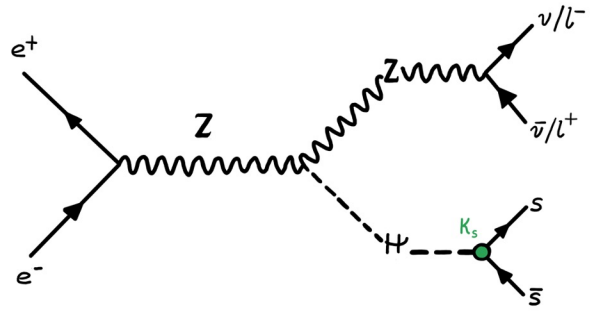

The Strange quark as a probe for New Physics

SM Higgs

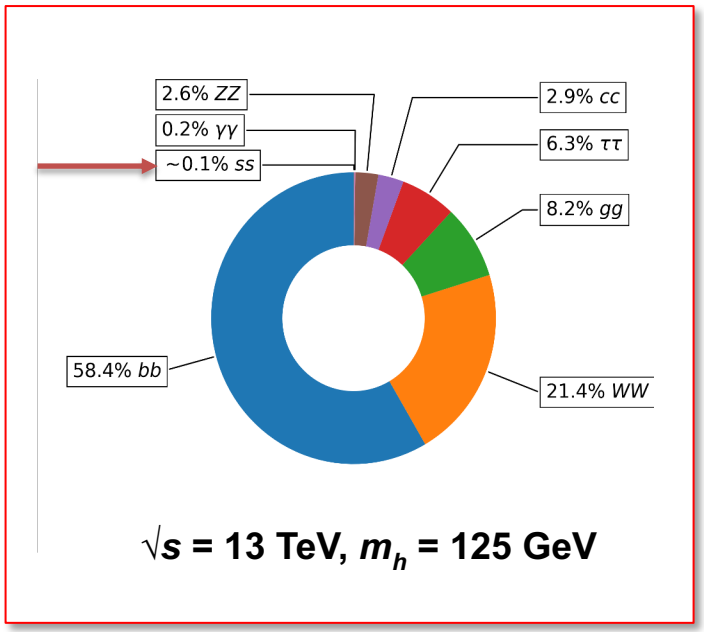

BSM Charged Higgs

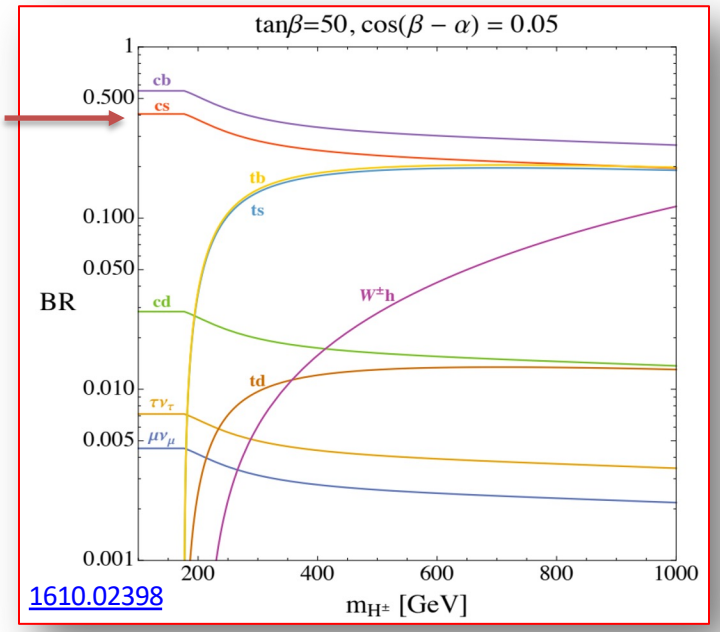

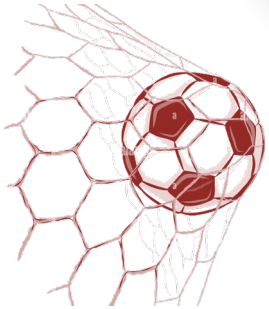

Assess the sensitivity of Higgs to strange couplings(*) at future Higgs Factories and study detector design enabling strange jet tagging

(*)many more SM analyses would benefit from strange tagging, e.g. $ee \to ss, Z \to ss, W \to cs$, etc!

Experimental Handles for Flavor Tagging

T. Tanabe's presentation

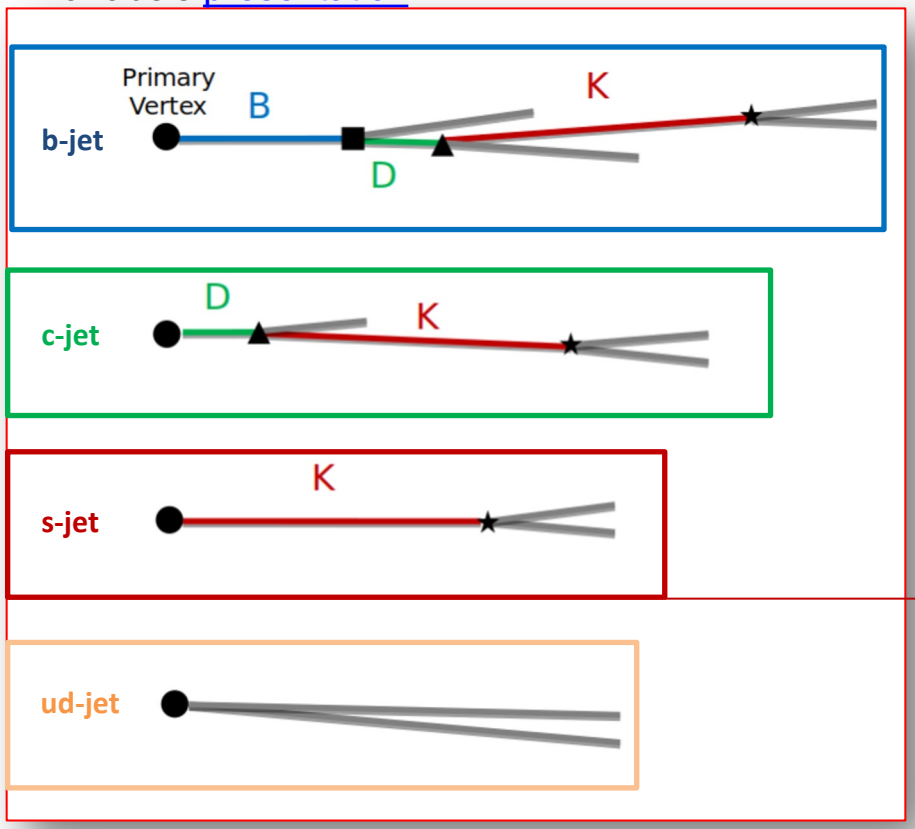

	# of secondary vertices (excluding V^0)	# of strange hadrons ($K^\pm$, K_L^0, K_S^0, Λ^0)
b	2	≥1
c	1	≥1
s	0	≥1
ud	0	0

Strange Hadron reconstruction

- $K^\pm$ [PID]
- $K_S^0 \rightarrow \pi^+\pi^-$ [Vertex] (BF ~69.2%)
- $\Lambda^0 \rightarrow p\pi^-$ [Vertex] (BF ~64%)
- K_L^0 [Particle Flow]

…and SLD actually measured strange hadrons from $Z \rightarrow s\bar{s}$!

See SLD A_s PRL 85 (2000), 5059

The *strange* features

2203.07535

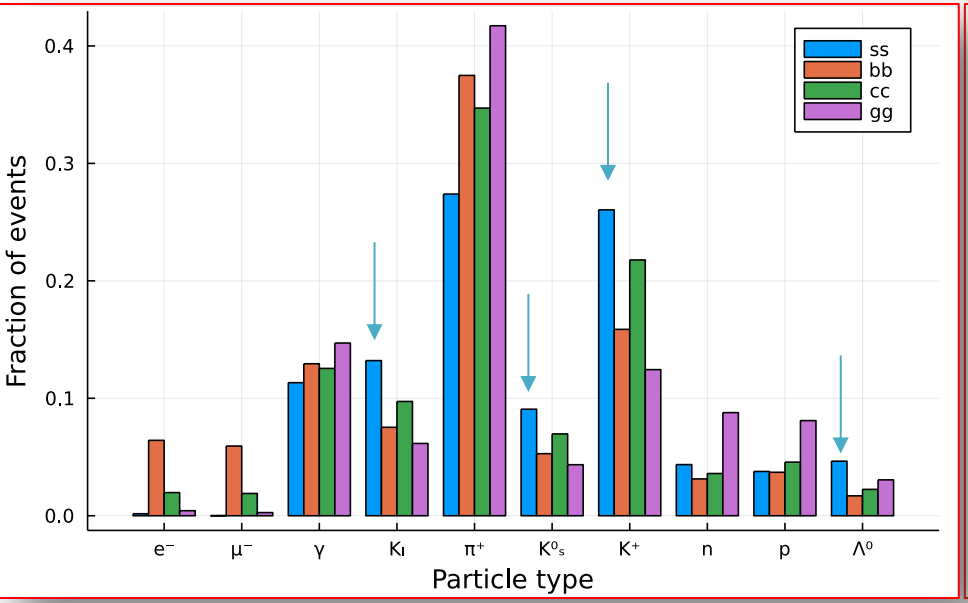

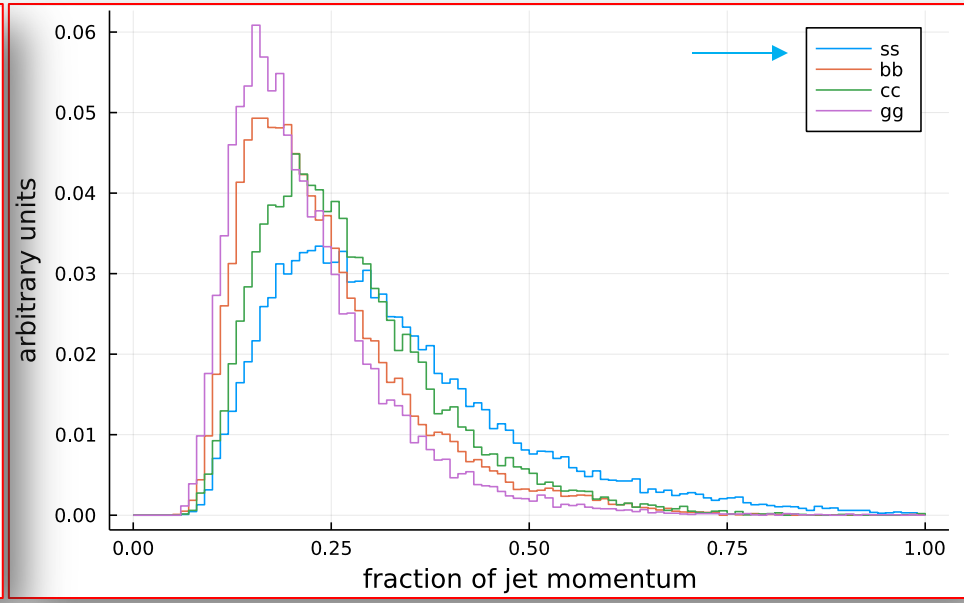

Particle Identification is crucial!

Need **π/K discrimination** over a momentum range of approximately
(0.2-0.7) x 0.5 x 125 ≅ **12 to 50 GeV**

Impact of PID on Strange Tagging

2203.07535

- Use a Recurrent Neural Net tagger for classifying jet-flavor, train on **full ILD(*) simulation** $(Z \to inv)(H \to q\bar{q}/gg)$ samples and include **per-jet level inputs** & **variables** on the **10 leading particles** in each jet, **including PDG-based PID** → general validity!

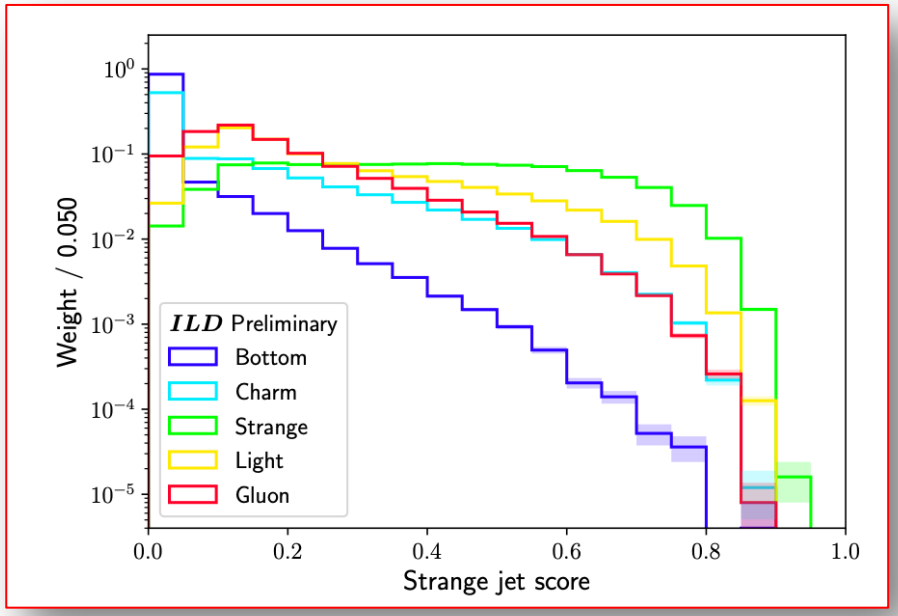

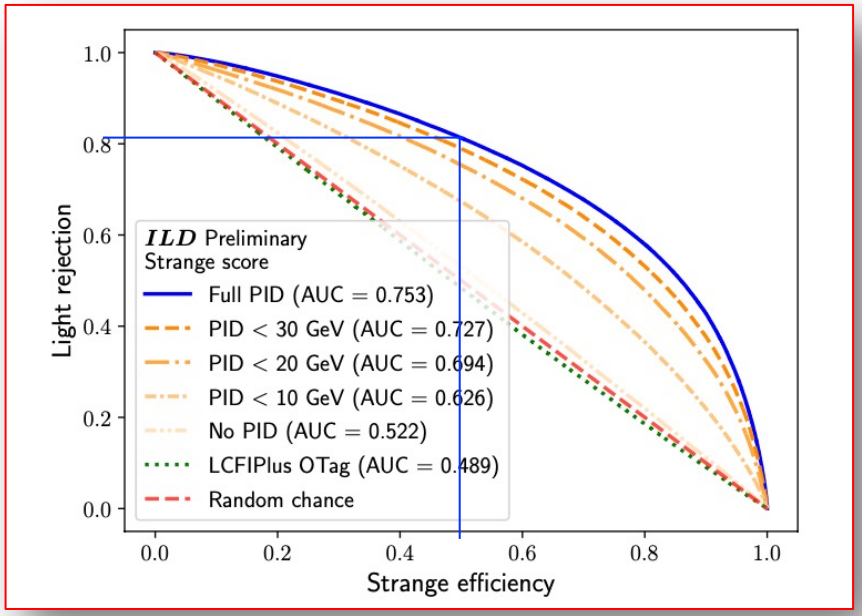

Good discrimination of *s*-jets from u/d- and *g*-jets

@50% s-jet tagging efficiency, >80% u/d-jet rejection with Full PID

(*) **ILD** = multi-purpose **International Large Detector** concept @ the International Linear Collider

Impact of PID on Strange Tagging

2203.07535

- Use a Recurrent Neural Net tagger for classifying jet-flavor, train on **full ILD simulation** $(Z \to inv)(H \to q\bar{q}/gg)$ samples and include **per-jet level inputs** & **variables** on the **10 leading particles** in each jet, **including PDG-based PID** → general validity!

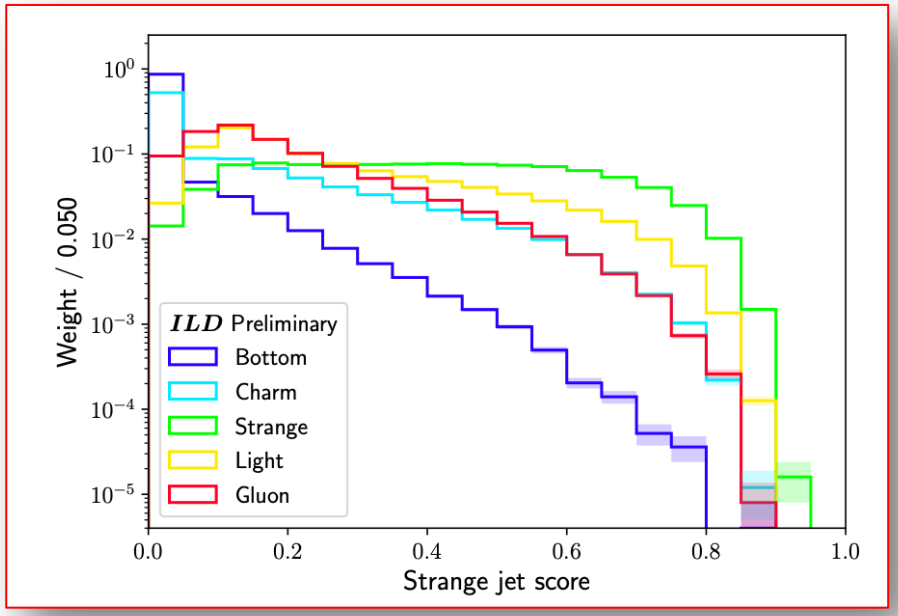

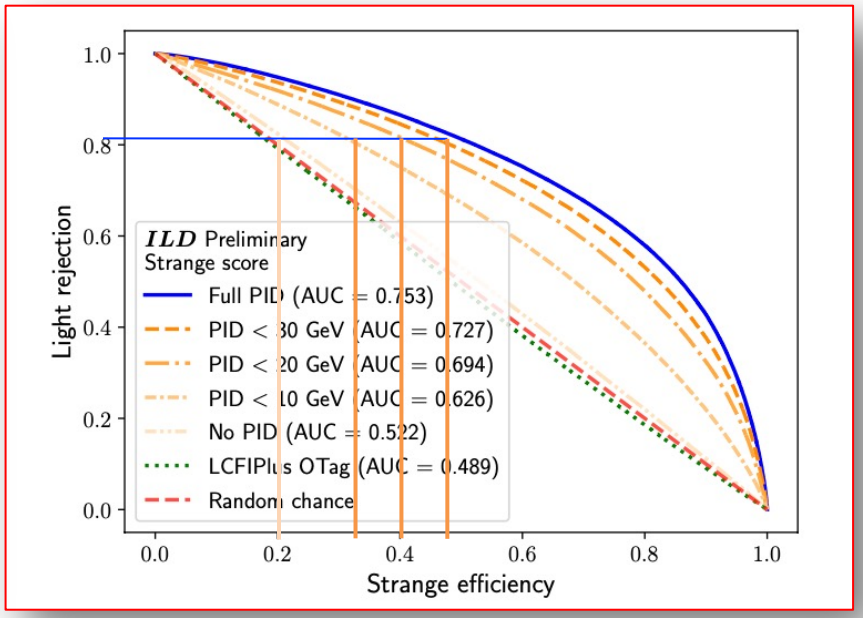

Good discrimination of *s*-jets from u/d- and *g*-jets

At fixed light rejection:
No PID to PID < 10 GeV: ~1.5x efficiency
No PID to PID < 20 GeV: ~2.0x efficiency
No PID to PID < 30 GeV: ~2.5x efficiency

A physics benchmark: $h \to s\bar{s}$ analysis @ the International Linear Collider

2203.07535

Foreseen to run at several $\sqrt{s}$, dedicated 250 GeV run for Higgs couplings studies

σ_H @ $\sqrt{s} = 250$ GeV ~ 200 fb (dominated by ZH production)

2000 fb^{-1} collected in 10y by ILC

→ $\sim$ 400k Higgs → $\sim$ 80 $h \to s\bar{s}$

But of course, new physics boosts these numbers!

$e^+e^- \rightarrow Zh \rightarrow \mu^+\mu^- h$

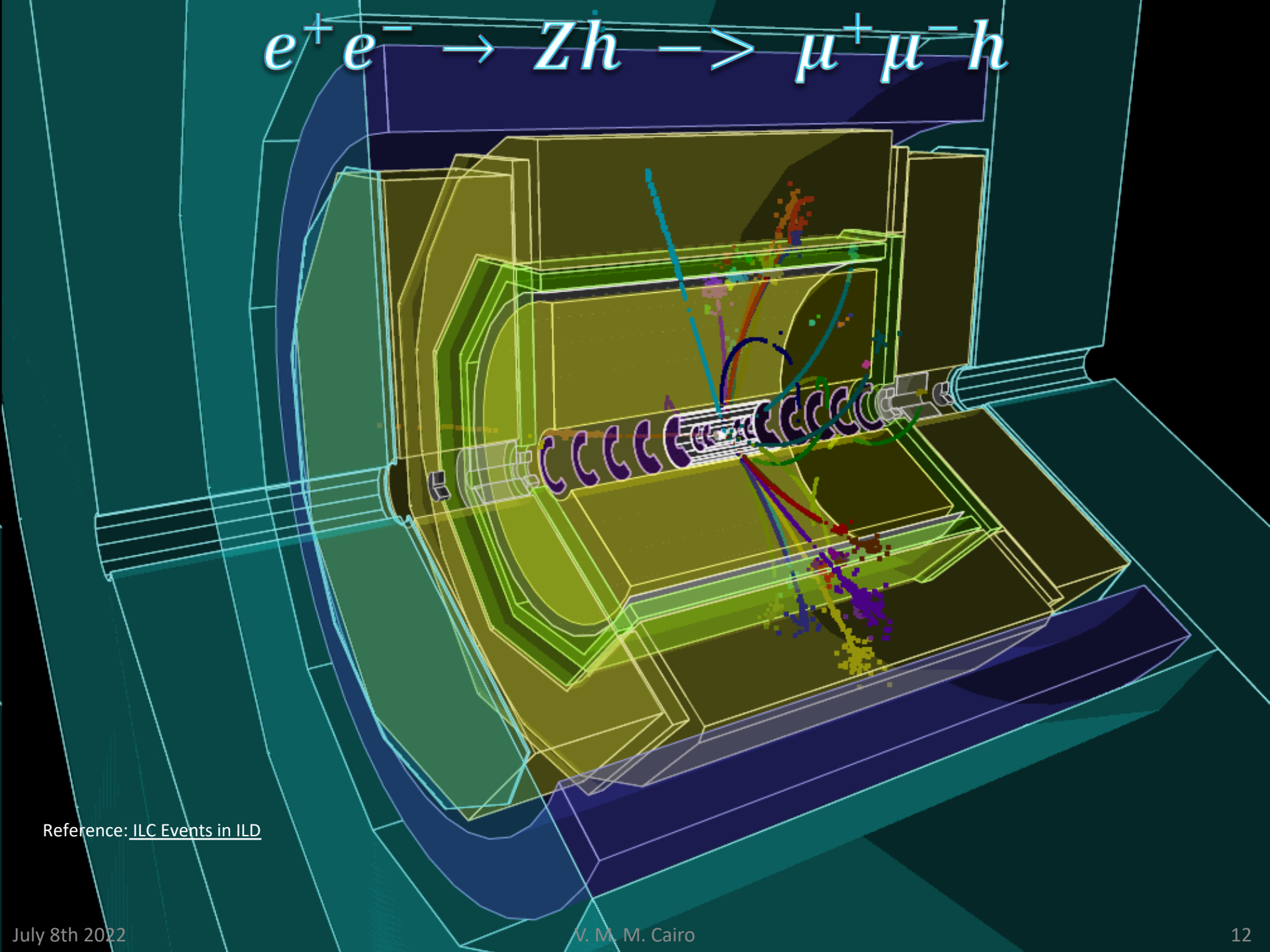

Reference: ILC Events in ILD

2203.07535

$h \to s\bar{s}$ analysis in a nutshell

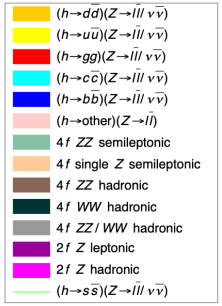

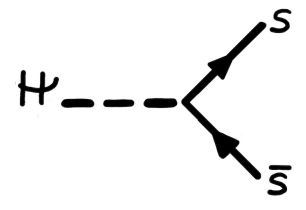

2 jets

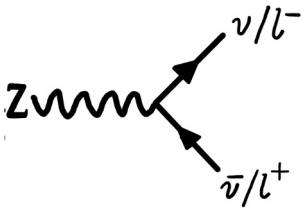

0 or 2 SFOS leptons

Object definition

Event selection

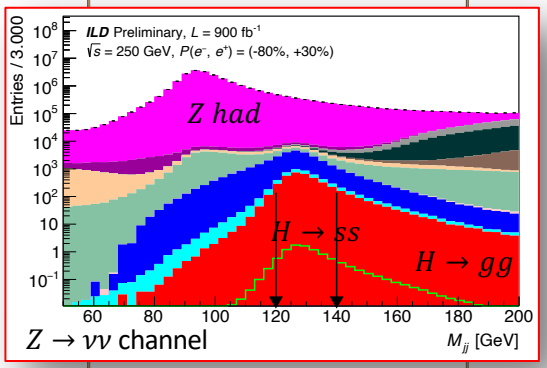

Cut-based approach, reject $ZH(!\,ss), V, VV$

Sum of

$jet_0 + jet_1$

strange tagging scores

Signal discriminant

s-Yukawa constraints

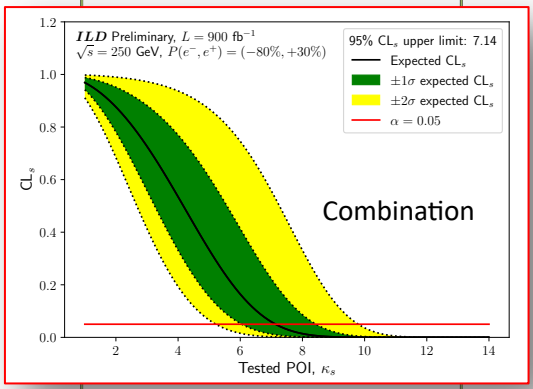

$k_s \lesssim 7$ x SM

- If we can tag strange jets, we can probe the **Higgs strange Yukawa** coupling…

But **we need π/K discrimination at high momenta**!

- This triggered recent studies of what may be possible with a system that pioneered particle ID: the **RICH**

Particle Identification techniques

R. Forty's slides

- Hadrons identified by their **mass**, determined from **momentum** and **velocity**
- Momentum inferred from radius of curvature in magnetic field, remaining question: measure the velocity
- The **ILD concept** has **intrinsic PID capabilities through dE/dx ionization + TOF from silicon wrappers**

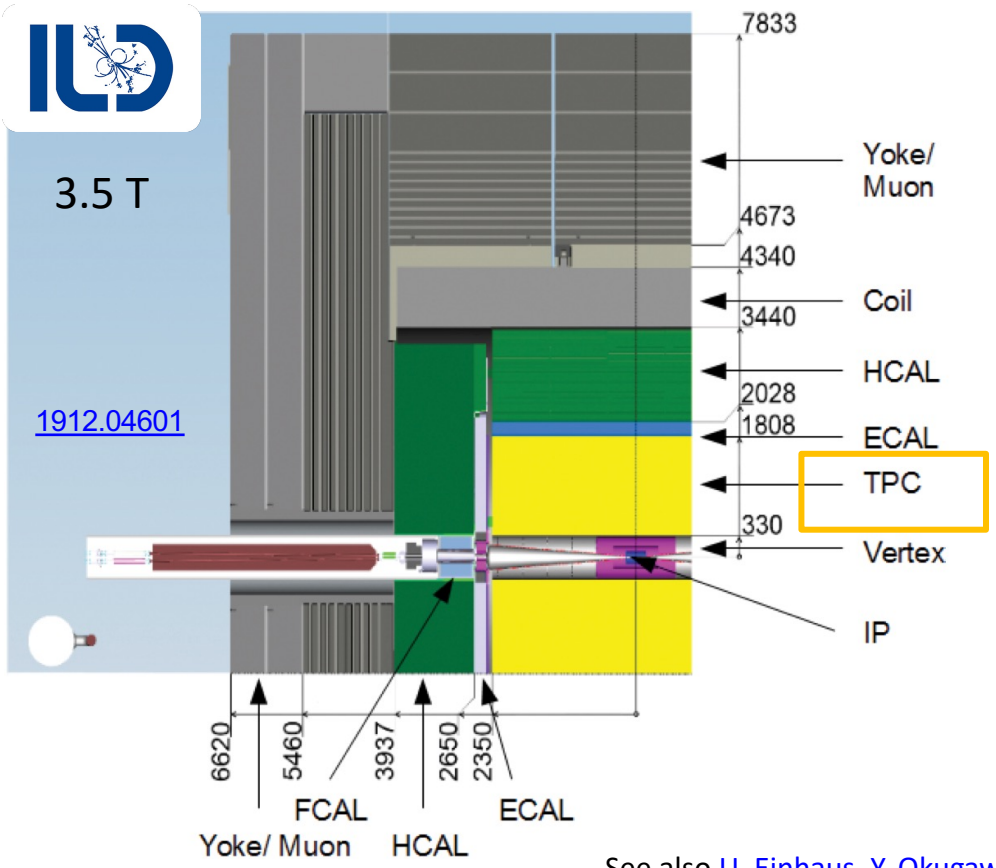

See also U. Einhaus, Y. Okugawa, B. Dudar's talks

Extending PID capabilities

2203.07535

TOF or dE/dX have great PID capabilities, but cover only the low momentum regime (unless very large tracker volumes are used)

TOF, dE/dX

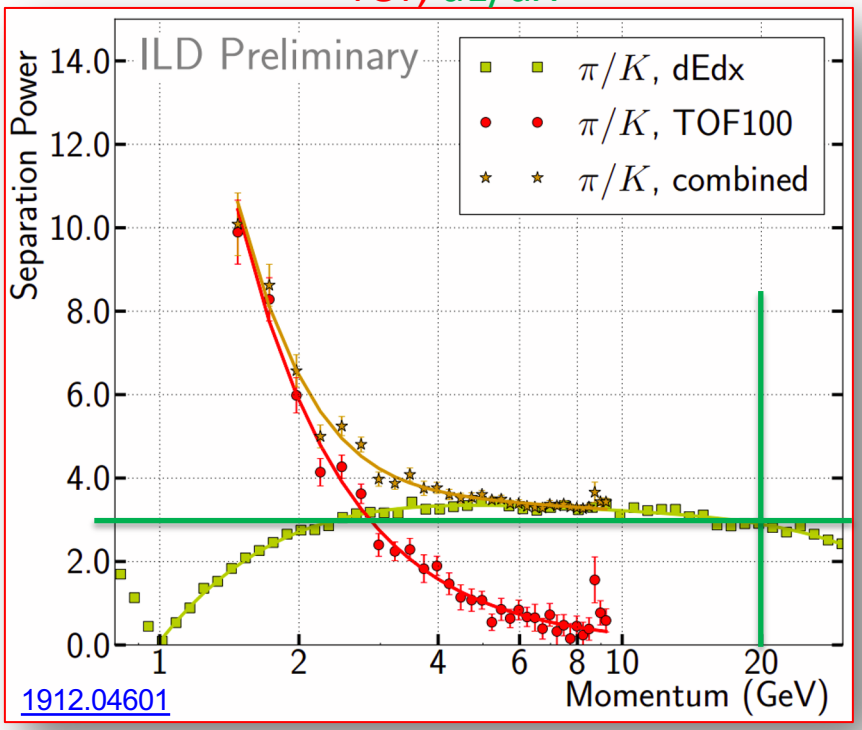

RICH

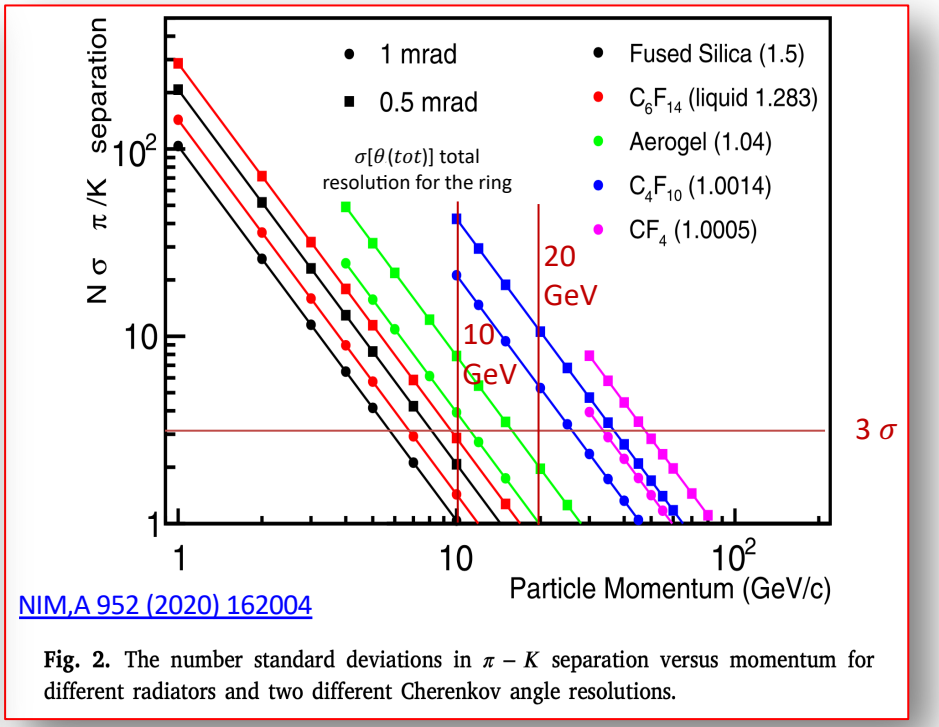

Fig. 2. The number standard deviations in $\pi - K$ separation versus momentum for different radiators and two different Cherenkov angle resolutions.

Ring Imaging Cherenkov Detectors (RICH) is a favourable approach at high momentum, but…

Will it be possible to accommodate a **compact RICH system** while preserving performance in tracking and calorimetry?

The past and the future RICH

2203.07535

- **Can a RICH work in limited (how limited?) radial space?**
  - Needs to be large enough to detect photons

Past

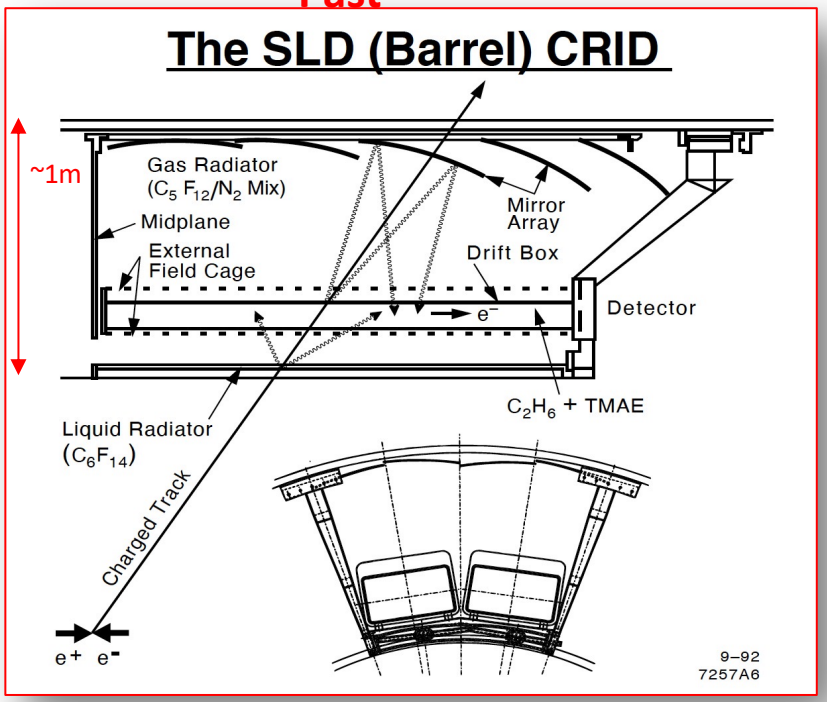

Future

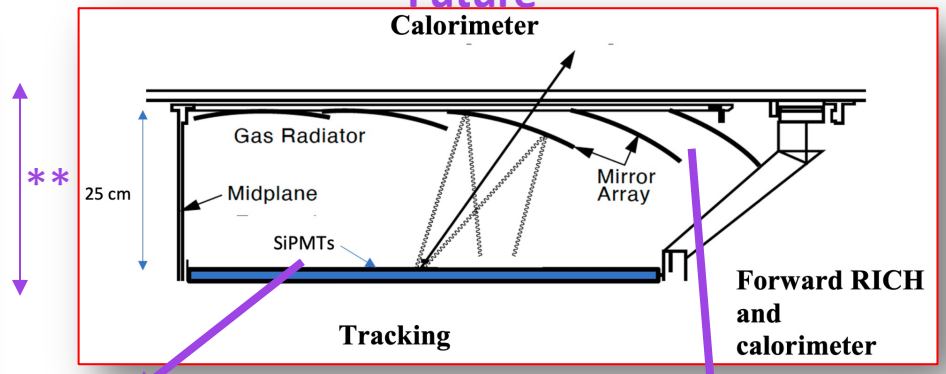

SiPMTs or new detector ideas!
See C. Damerell's article

Extremely thin but excellent optical quality mirrors

** Needed radiator thickness will evolve downwards, as Quantum Efficiency of photodetectors advances

- **Past** → **Future**: Much **smaller** radial length, **SiPMTs** rather than TPCs with TMAE for photon detection improve PID by a factor of 2
- **Many parameters to investigate!**

Compact Gaseous RICH with SiPMTs

2203.07535

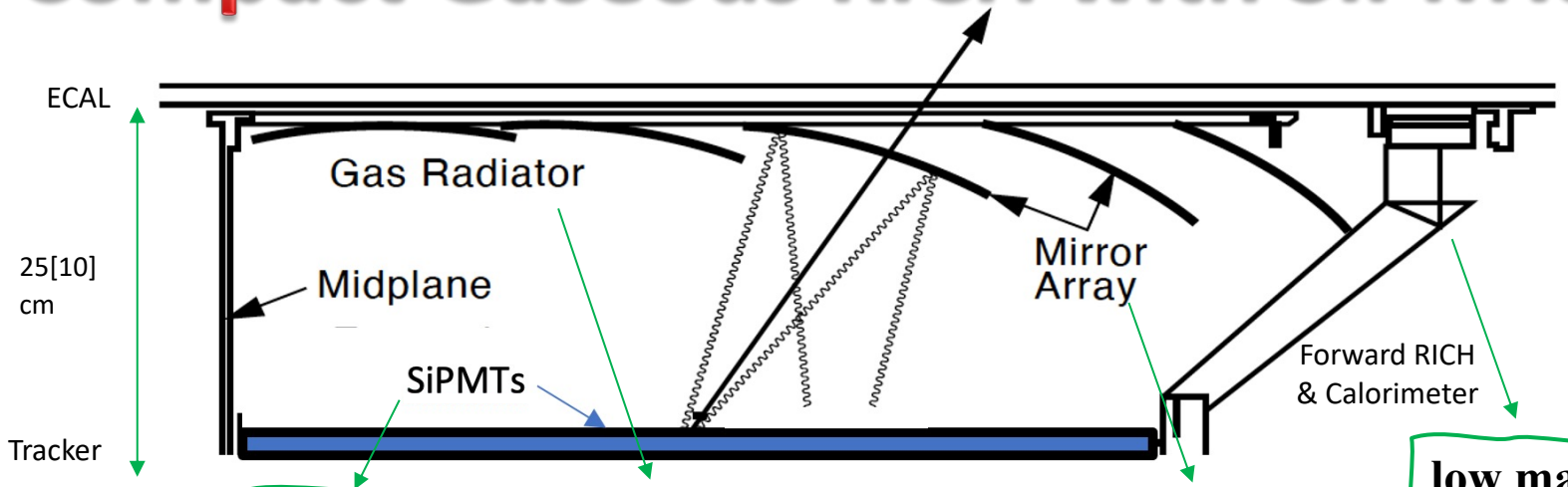

Fast timing device (<100 ps) to provide ToF covering the lower p range and complementing the RICH

Pure C_4F_{10} at 1 bar (boiling point -1.9 C at 1 bar, good refraction index)

Beryllium with reflective coating

low mass carbon-composite material for the structure

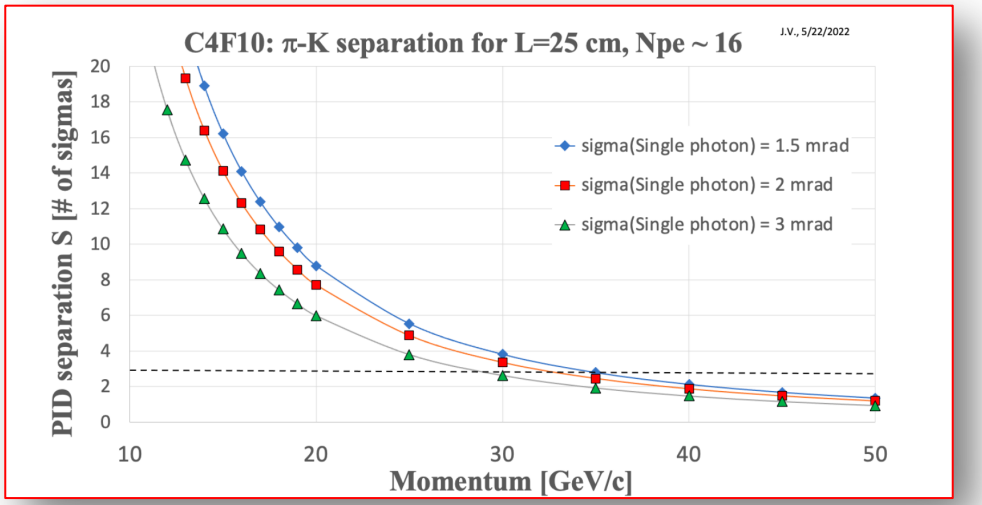

Can reach 3σ π/K separation up to 30 GeV with state-of-the-art technology!

The importance of *strange* science

2203.07535

- Many unexplored physics benchmarks rely on **strange tagging**, in turn enabled by $\boldsymbol{\pi/K}$ **PID at high momenta**
  - Higgs *& friends* Factories: **Z, W, top, flavor physics in general…** (see R. Forty's talk)
- Ordinary matter composed by electron and light quarks
  - **none of the Higgs boson couplings to such particles has been verified yet!**
- Testing Yukawa universality: **key benchmark** for future Higgs factories
- The most stringent constraints on the **strange Yukawa** have been derived via a direct SM $\boldsymbol{h \to s\bar{s}}$ search: phase space for new physics reduced to $\boldsymbol{k_s \lesssim 7\ x\ SM}$

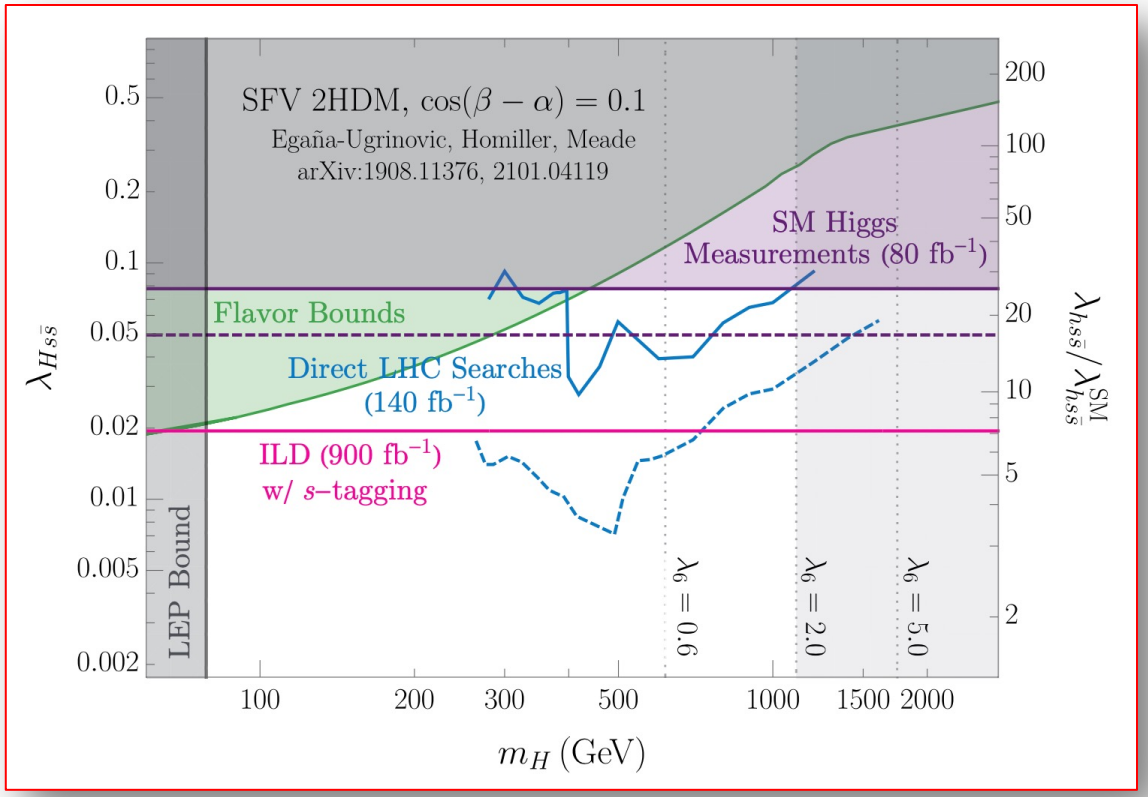

Illustrations by F. Cairo

Wrap-up & Conclusions

Probing the Strange Yukawa coupling:
a challenge and an opportunity at Future Colliders

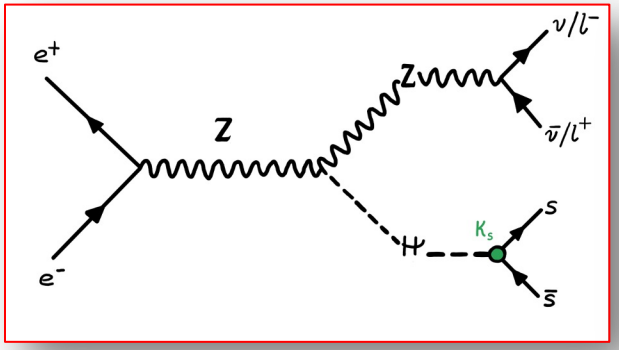

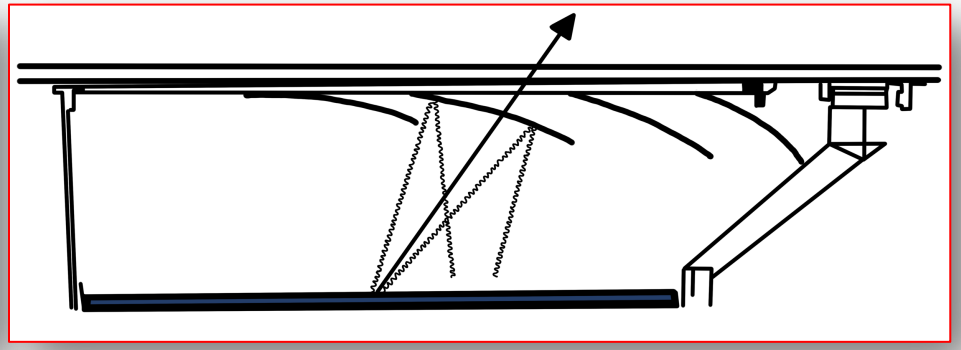

Exciting science ahead to solve **some of the yet-to-be answered questions** in Particle Physics

Interplay between **detector design, performance & analysis techniques** is of paramount importance!

Thanks for your attention!

Valentina Maria Martina Cairo

CERN

Extra slides

Future Colliders

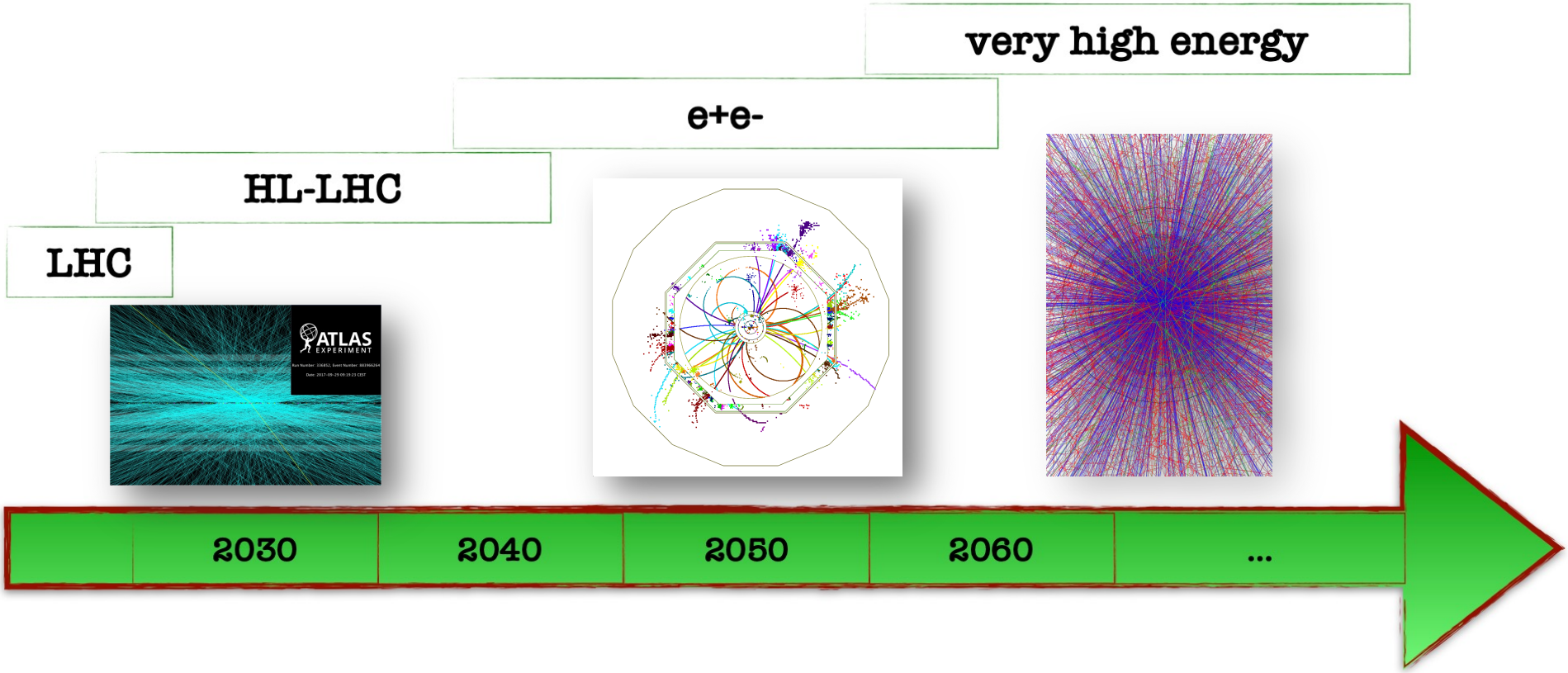

- pp: high energy, large statistics → ideal e.g. for rare Higgs searches
- e^+e^-: clean environment, initial states well defined → ideal for precision measurments and for probing light Yukawas

NN Architecture

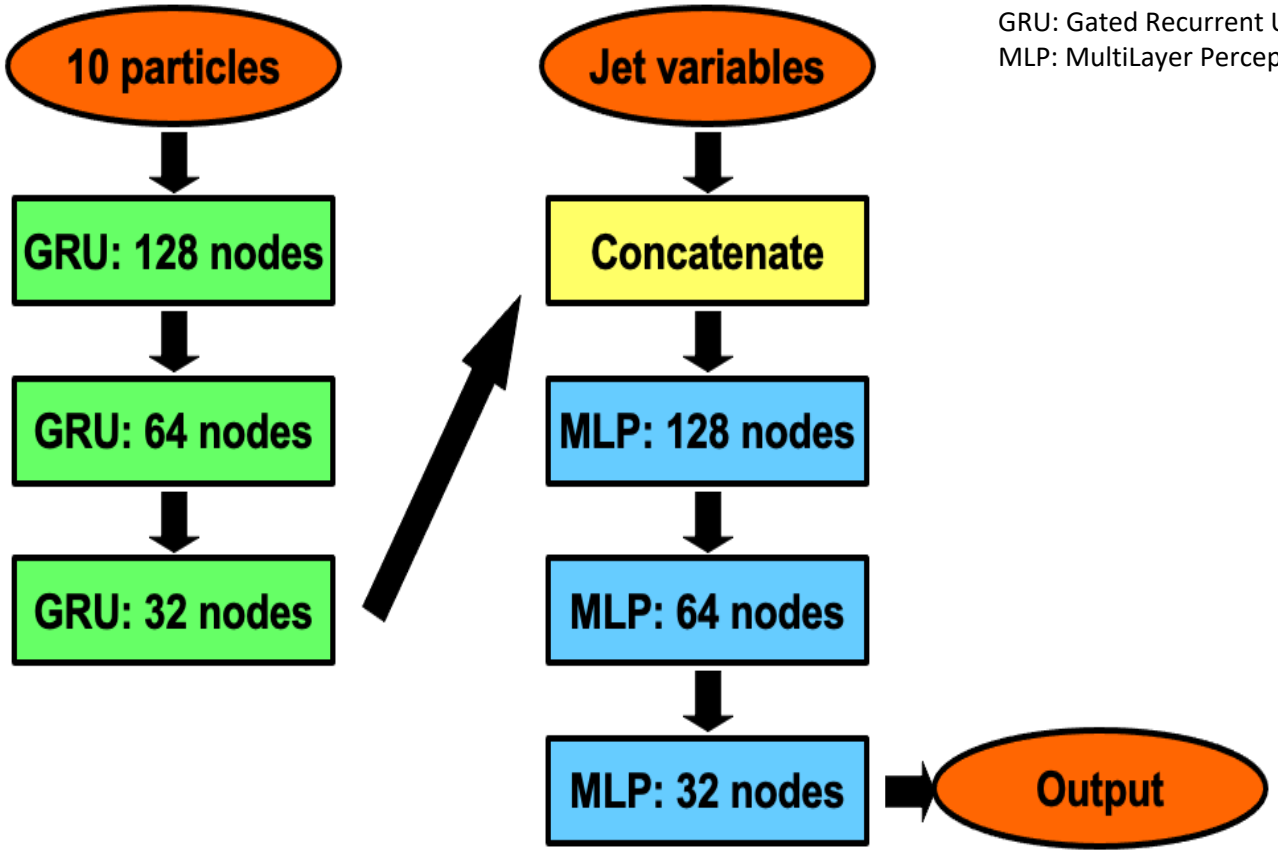

GRU: Gated Recurrent Units
MLP: MultiLayer Perceptron

NN Inputs in ILD

The training is performed on the $Z(\rightarrow \nu\bar{\nu})h(\rightarrow q\bar{q}/gg)$ samples from table 2. All events are required to have $N_{\text{jets}} \geq 2$ and $N_{\text{leptons}} = 0$. The training is performed using only one jet per event, where the leading or subleading momentum jet is randomly chosen. Per process, 250,000 raw MC events are used – additionally, the $h \rightarrow u\bar{u}$ and $h \rightarrow d\bar{d}$ processes are combined into a single class, $h \rightarrow$ light.

As input to the ANN, several jet-level variables are chosen:

Jets

- kinematics: momentum p, pseudorapidity η, polar angle ϕ, and mass m;
- LCFIPlus tagger results: b- ("BTag"), c- ("CTag"), and o-tag ("OTag") scores as well as jet category;
- number of Particle Flow Objects (PFOs – these are the particles which are grouped into the jet).

In addition to jet-level variables, it is prudent to include variables at the level of the PFOs contained within the jet. The 10 leading momentum particles contained within the jet have their kinematics redefined relative to the jet's axis and their momentum and mass scaled by the momentum of the jet. Per-particle, the following variables are also chosen as inputs:

Tracks

- kinematics: p, η, ϕ, and m;
- charge q;
- truth likelihoods: $L(e^{\pm})$, $L(\mu^{\pm})$, $L(\pi^{\pm})$, $L(K)$, $L(p^{+})$.

The ILD detector will provide PID information per PFO, including electron ($e^{\pm}$), muon ($\mu^{\pm}$), pion ($\pi^{\pm}$), kaon (K), and proton (p^{+}) likelihoods, L. However, the reconstructed likelihoods utilising the dE/dx and TOF information were not available in the inputs at the time of the study. *Truth* likelihoods are assigned instead, representing a best-case scenario in terms of PID. The 5 truth likelihoods are assigned a binary number by comparing the absolute value of PDG ID [39] of the PFO to the PDG ID(s) of each particle class:

PID

- electrons: 11;
- muons: 13;
- pions: 211;
- kaons: 310, 321, and 3122 (includes V^0's: K_s^0 and Λ^0);
- protons: 2212;

where 1 is assigned if one of the PDGs match and 0 is assigned otherwise.

Impact of PID on Strange Tagging

2203.07535

- Use a Recurrent Neural Net tagger for classifying jet-flavor, train on **full ILD simulation** $(Z \to inv)(H \to qq/gg)$ samples and include **per-jet level inputs** & **variables** on the **10 leading particles** in each jet, **including PDG-based PID** → general validity!

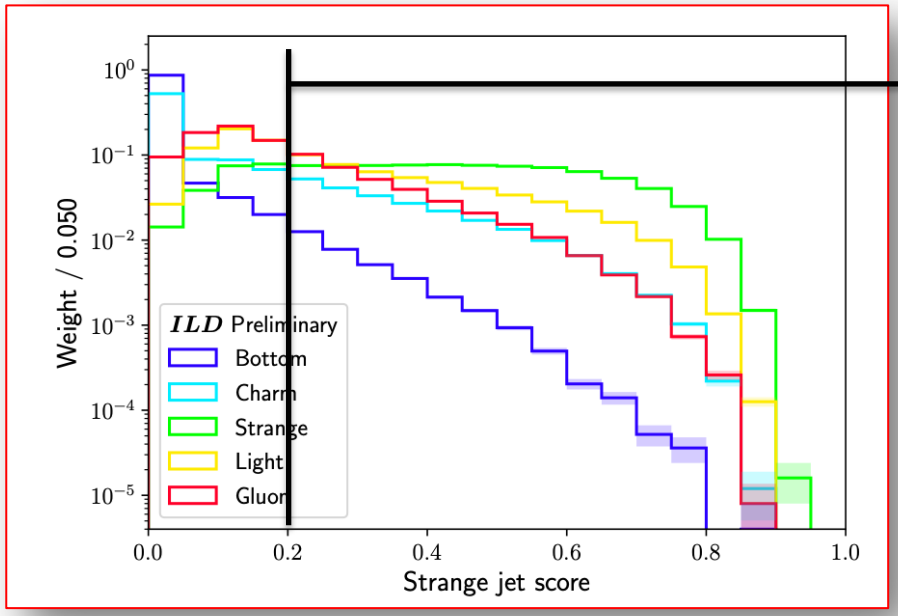

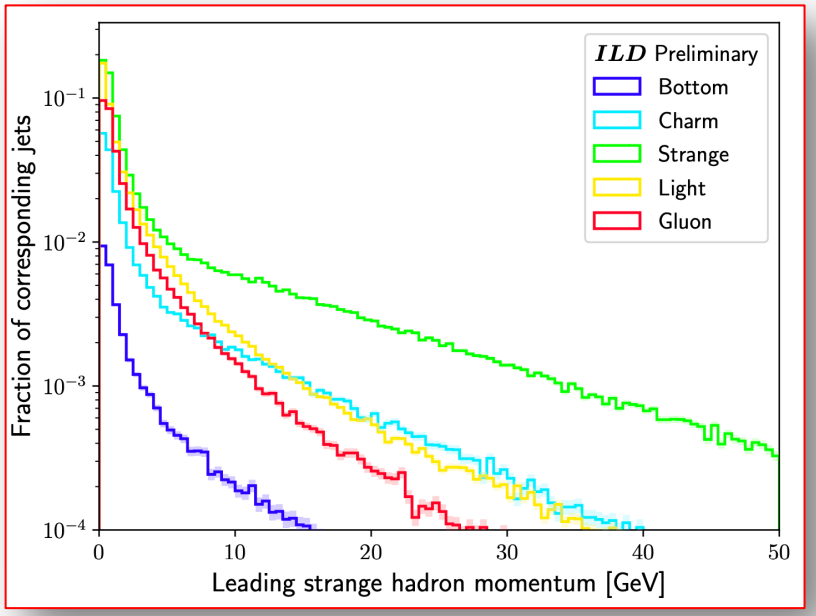

The tighter the cut on the s-tag score,
the more energetic the leading strange hadron!

Particle Identification techniques

R. Forty's slides

- Hadrons are identified by their **mass**, in turn determined by combining **momentum** and **velocity**
- Assuming that momentum is inferred from radius of curvature in magnetic field, the remaining issue is to measure the velocity

  - Can be determined via:

    - **Time-of-flight** (TOF)

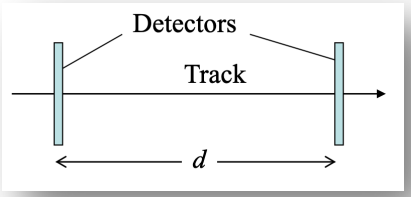

    - **Ionization losses** (dE/dx or dN/dx)

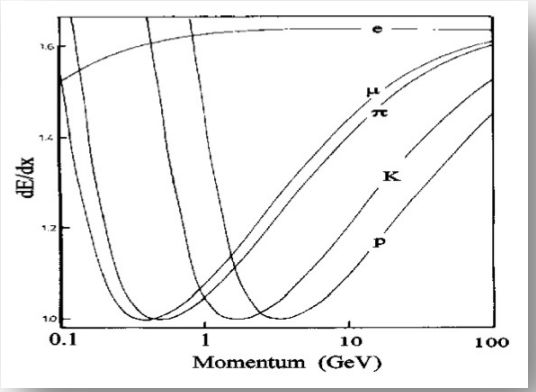

    - **Transition radiation**

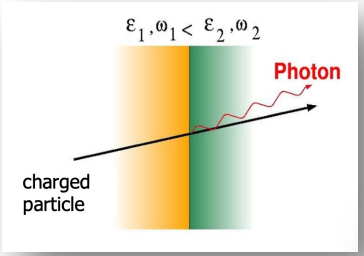

    - **Cherenkov radiation**

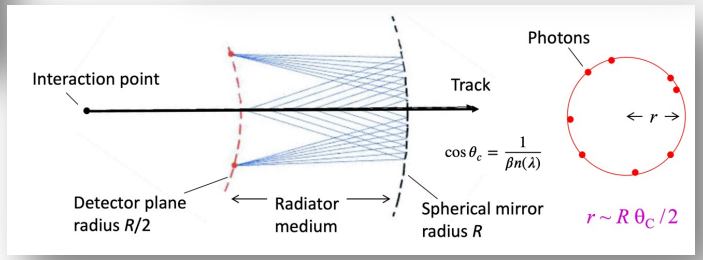

N.B. Detection of photons is needed by many of the detectors performing particle ID.
Requirements: single photon sensitivity, high efficiency, good spatial granularity

Two examples:
IDEA @ FCC-ee & ILD @ ILC

IDEA @ FCC-ee

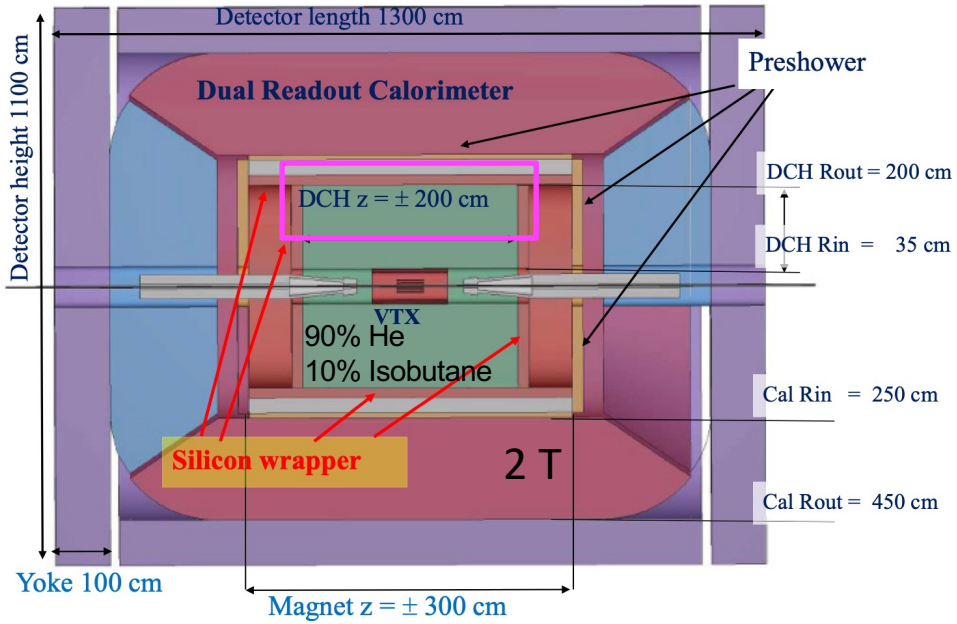

e2019-900045-4

ILD @ ILC

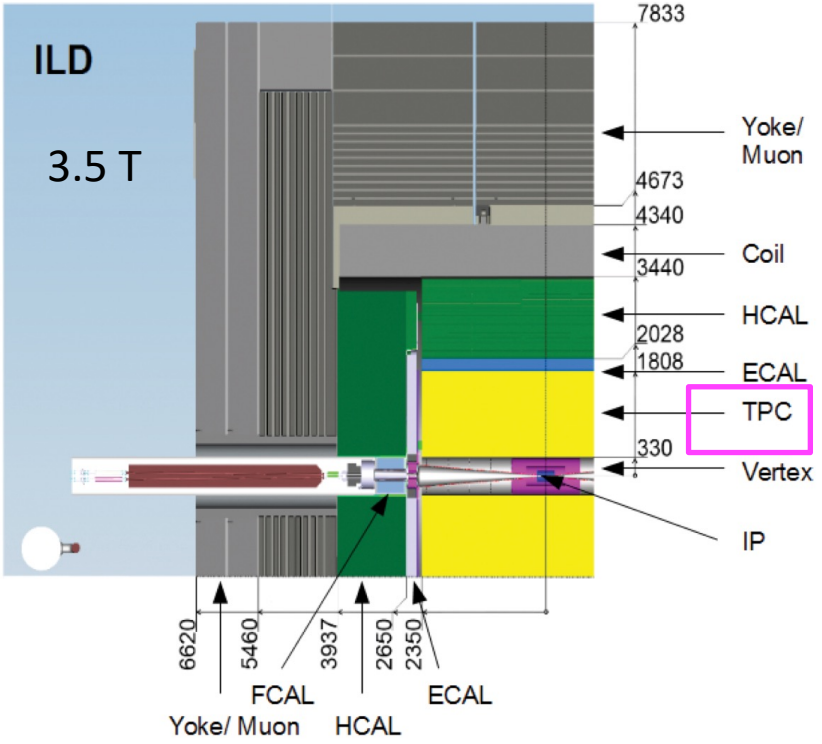

1912.04601

Two examples: IDEA @ FCC-ee & ILD @ ILC

IDEA @ FCC-ee

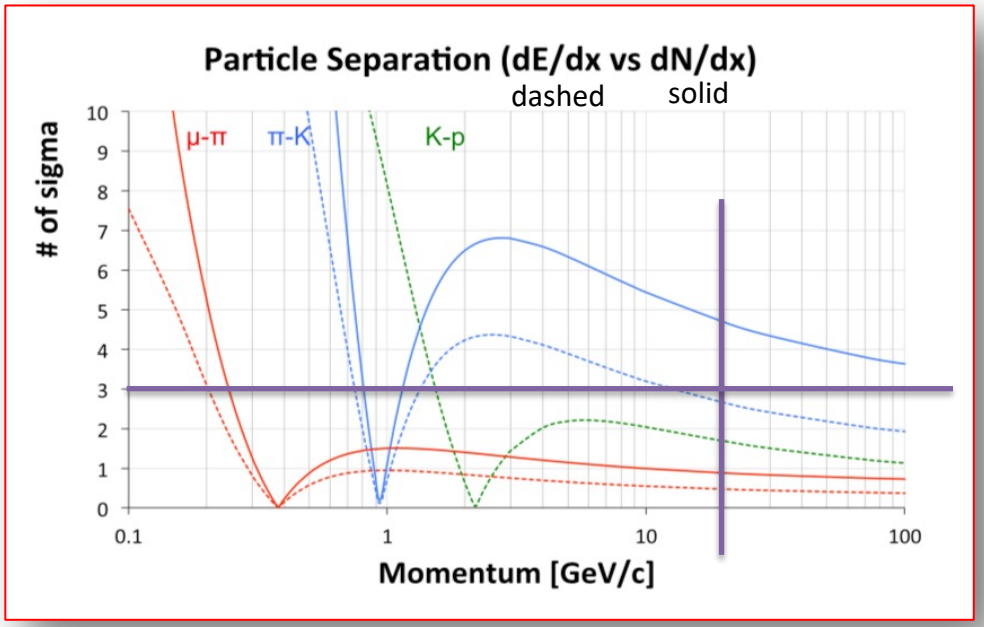

Analitical calculations

e2019-900045-4

ILD @ ILC

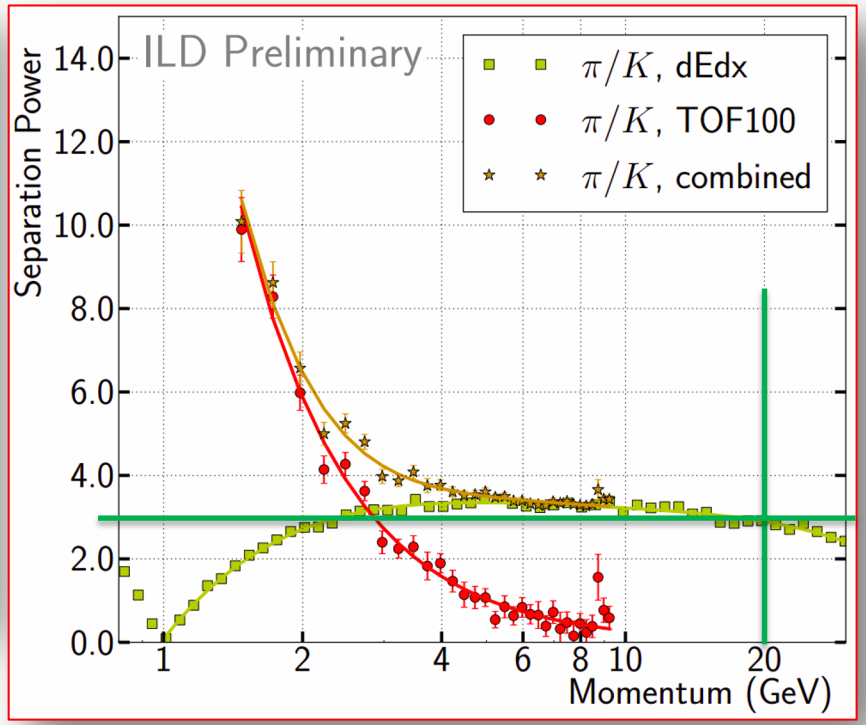

1912.04601

Comparable dE/dx performance at e.g. 20 GeV, boost from dN/dx

2202.03285

Strange Tagging with IDEA

- Use a Graph Neural Net *ParticleNetIdea*: jets represented as an un-ordered set of particles
- Train on $(Z \to inv)(H \to qq/gg)$ samples, **per-jet and per-particle level inputs** & **variables** (kinematics, displacement, identification)
- TOF and dN/dx (**3σ < 30 GeV**) considered
- **Fast Simulation and Fast Tracking**

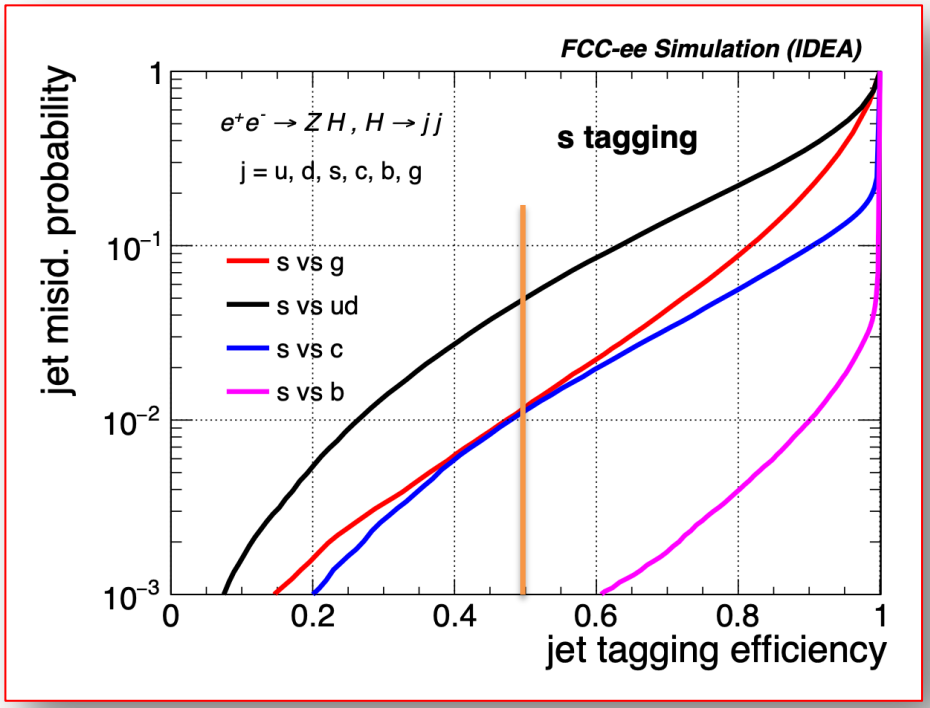

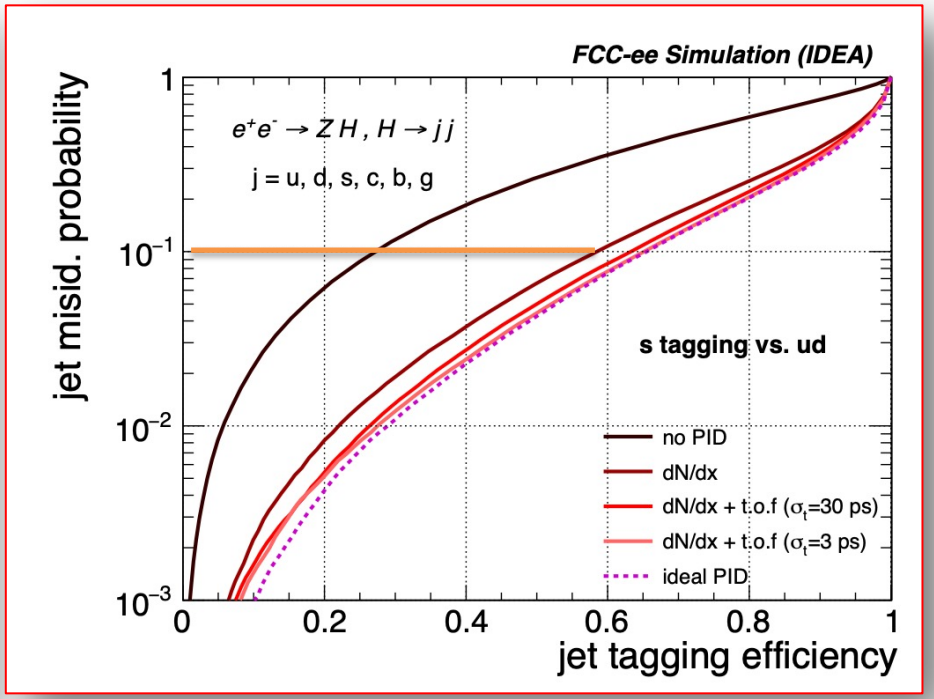

No PID to PID with dN/dx → at fixed mistag, **efficiency doubles**

PID Technology comparison

3σ separation for π/K				
dE/dx in silicon	TOF via Fast Timing in silicon envelopes or calorimetry	dE/dx in Time Projection or Drift Chambers	dN/dx	RICH
$\lesssim$ 5 GeV	$\lesssim$ 5 GeV	$\lesssim$ 30 GeV (scales with volume)	O(tens of GeV)	O(tens of GeV)

Event Selection

Table 3: Kinematic selections for $Z \to \nu\bar{\nu}$ and $Z \to \ell\ell$ channels of the $h \to s\bar{s}$ analysis. The selections are grouped into categories serving specific purposes.

Category	Selection	$Z \to \nu\bar{\nu}$	$Z \to \ell\ell$
Object counting	Number of leptons, N_{leptons}	0	≥ 2
	Number of jets, N_{jets}	≥ 2	≥ 2
	Leading 2 leptons are SFOS[2]	–	True
$2f$ Z rejection	Leading jet momentum, p_{j_0}	$\in [40, 110]$ GeV	$\in [60, 110]$ GeV
	Subleading jet momentum, p_{j_1}	$\in [30, 80]$ GeV	$\in [30, 75]$ GeV
	Dijet mass, M_{jj}	$\in [120, 140]$ GeV	$\in [115, 145]$ GeV
	Dijet energy, E_{jj}	$\in [125, 155]$ GeV	$\in [130, 160]$ GeV
	Missing mass, M_{miss}	$\in [75, 120]$ GeV	–
	Dijet/missing-p^{μ} angular separation, $\Delta R_{jj,\text{miss}}$[3]	$\in [3.1, 4.0]$[4]	–
	Dijet azimuthal separation, $\Delta\phi_{jj}$	> 1.25	> 1.75
	Leading lepton momentum, p_{ℓ_0}	–	$\in [40, 90]$ GeV
	Subleading lepton momentum, p_{ℓ_1}	–	$\in [20, 60]$ GeV
	Dilepton mass, $M_{\ell\ell}$	–	$\in [70, 100]$ GeV
	Dilepton energy, $E_{\ell\ell}$	–	$\in [85, 115]$ GeV
$h \to b\bar{b}/c\bar{c}$ rejection	Leading jet LCFIPlus BTag score, $\text{score}_b^{j_0}$	< 0.20	< 0.1
	Subleading jet LCFIPlus BTag score, $\text{score}_b^{j_1}$	< 0.20	< 0.1
	Leading jet LCFIPlus CTag score, $\text{score}_c^{j_0}$	< 0.35	< 0.3
	Subleading jet LCFIPlus CTag score, $\text{score}_c^{j_1}$	< 0.35	< 0.3
$4f$ VV rejection	$2 \to 3$ jet transition variable, y_{23}	< 0.010	< 0.050
	$2 \to 3$ jet transition variable, y_{34}	< 0.002	< 0.005
$h \to gg$ rejection	Number of PFOs in event, $N_{\text{PFOs}}^{\text{event}}$	$\in [30, 60]$	$\in [20, 80]$
	Number of PFOs in leading jet, $N_{\text{PFOs}}^{j_0}$	$\in [10, 40]$	$\in [5, 50]$
	Number of PFOs in subleading jet, $N_{\text{PFOs}}^{j_1}$	$\in [9, 37]$	$\in [5, 50]$

Cut flows

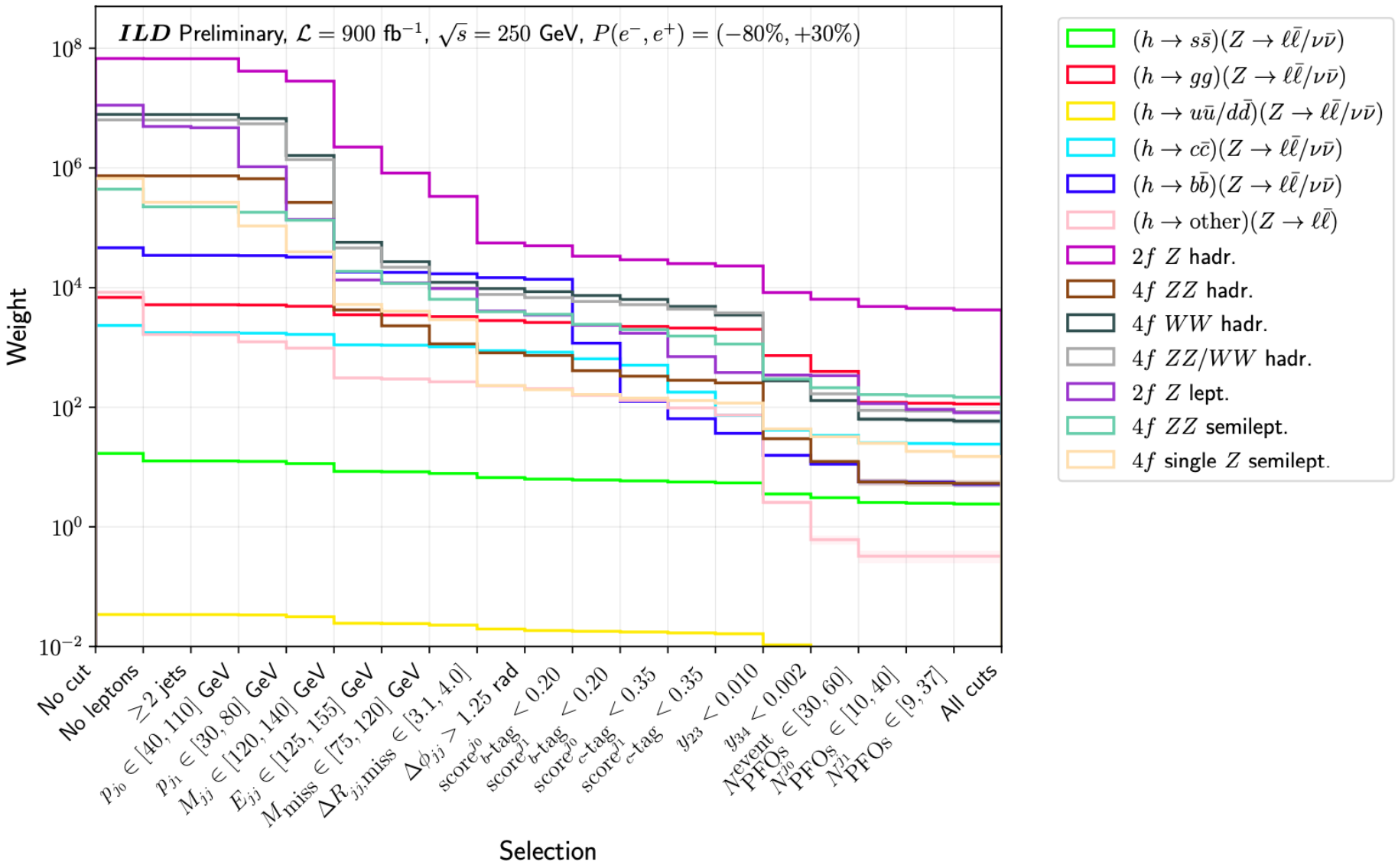

(a) $Z \to \nu\bar{\nu}$ channel

Cut flows

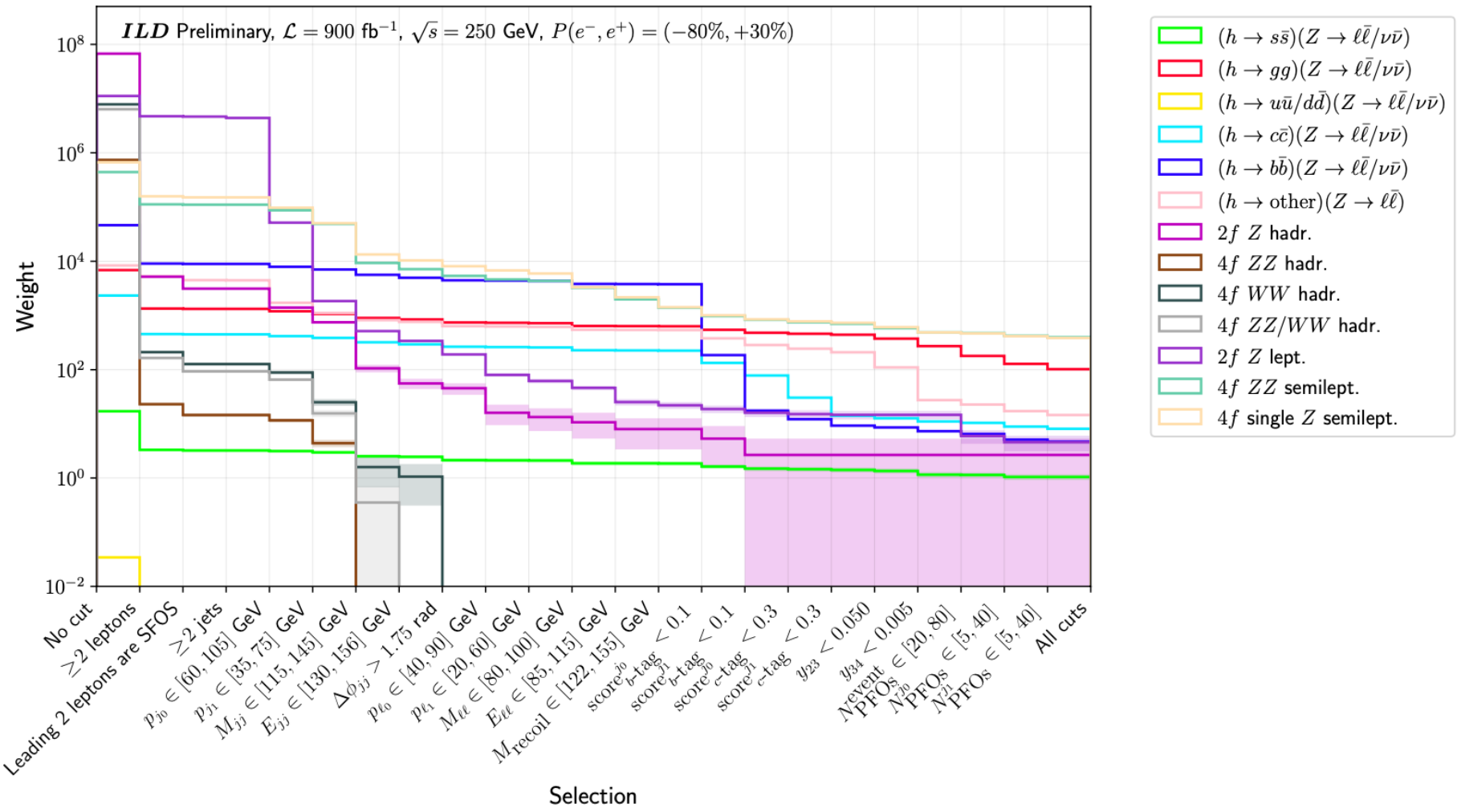

(b) $Z \to \ell\bar{\ell}$ channel

Strange discriminant

2203.07535

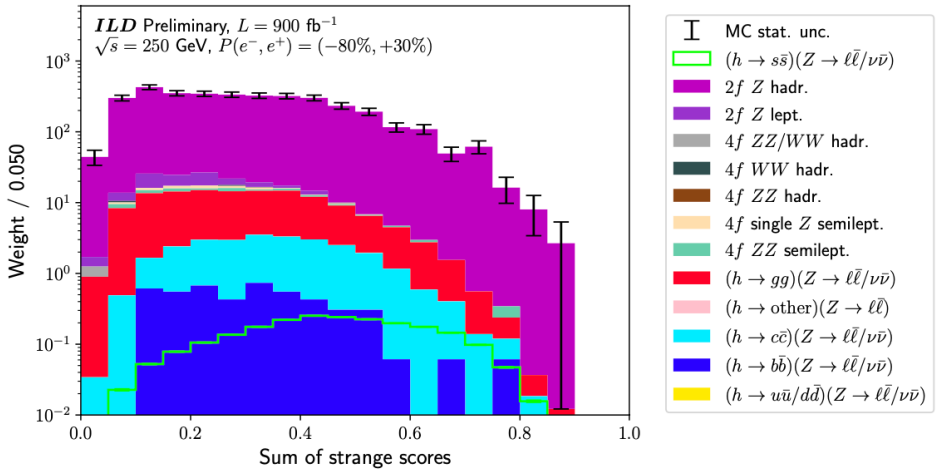

(a) $Z \to \nu\bar{\nu}$ channel

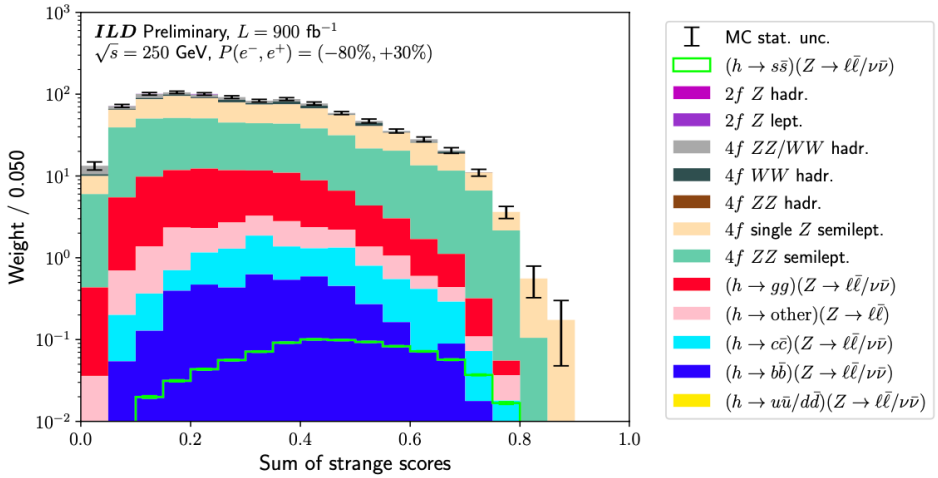

(b) $Z \to \ell\bar{\ell}$ channel

Figure 19: Fit discriminants for each channel of the SM $h \to s\bar{s}$ analysis, Eq. 8. Each histogram is produced at the level of the last selection of their respective channel in Table 3. The error bars represent the MC statistical uncertainties. The sum-of-weights per process is normalised to the SM cross section. N.B. the $h(\to s\bar{s})Z(\to \ell\bar{\ell}/\nu\bar{\nu})$ signal is unstacked.

Strange discriminant

2203.07535

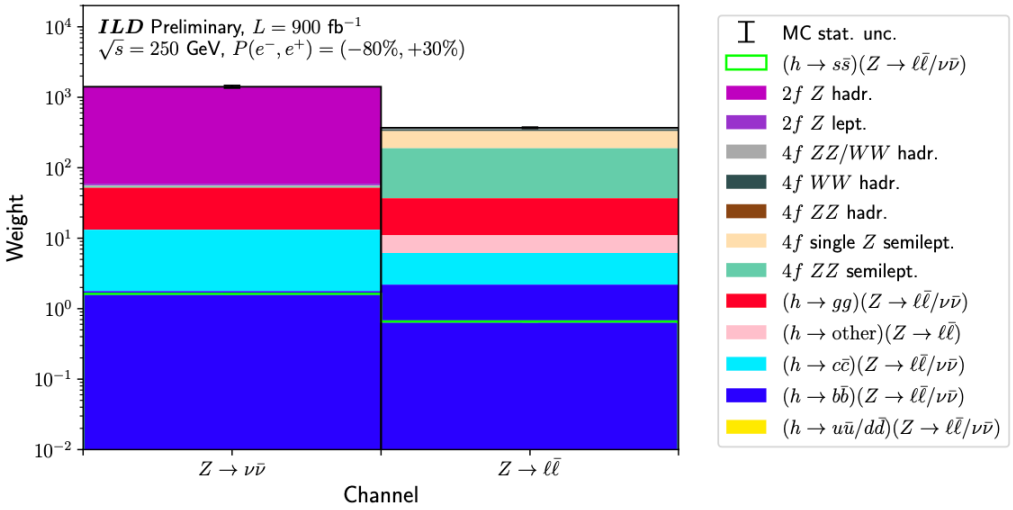

Figure 21: Yields in the signal regions for the $Z \to \nu\bar{\nu}$ and $Z \to \ell\bar{\ell}$ channels, obtained by applying selections of >0.35 on the respective discriminants shown in Fig. 19. The error bars represent the MC statistical uncertainties, and the sum-of-weights per process is normalised to the SM cross section. N.B. the $h(\to s\bar{s})Z(\to \ell\bar{\ell}/\nu\bar{\nu})$ signal is unstacked.

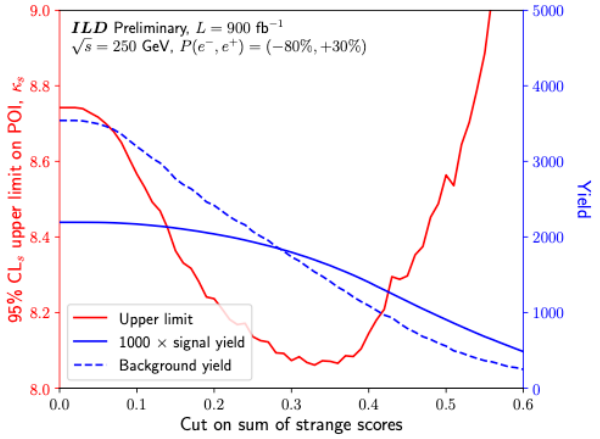

(a) $Z \to \nu\bar{\nu}$ channel

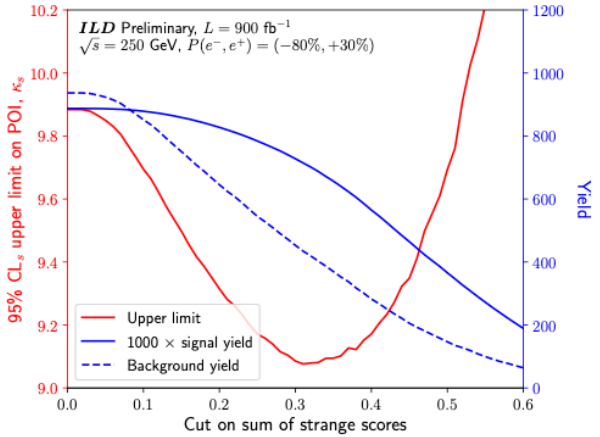

u/d Yukawa couplings

2203.07535

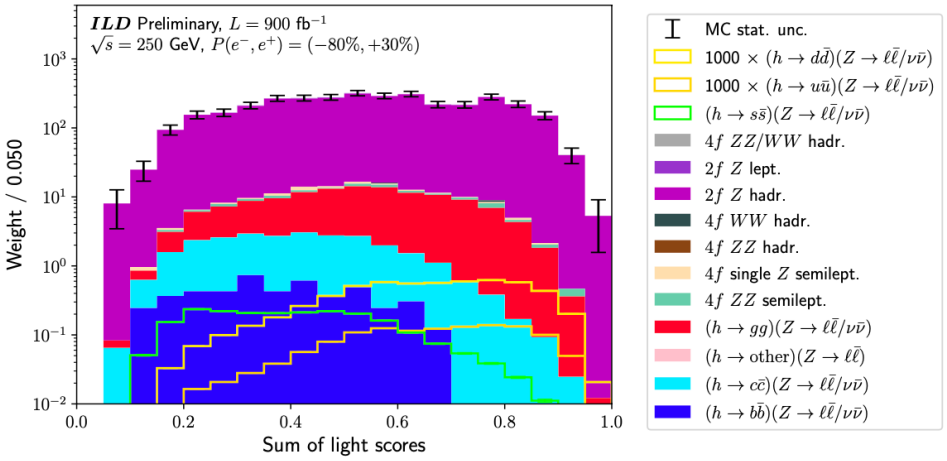

(a) $Z \to \nu\bar{\nu}$ channel

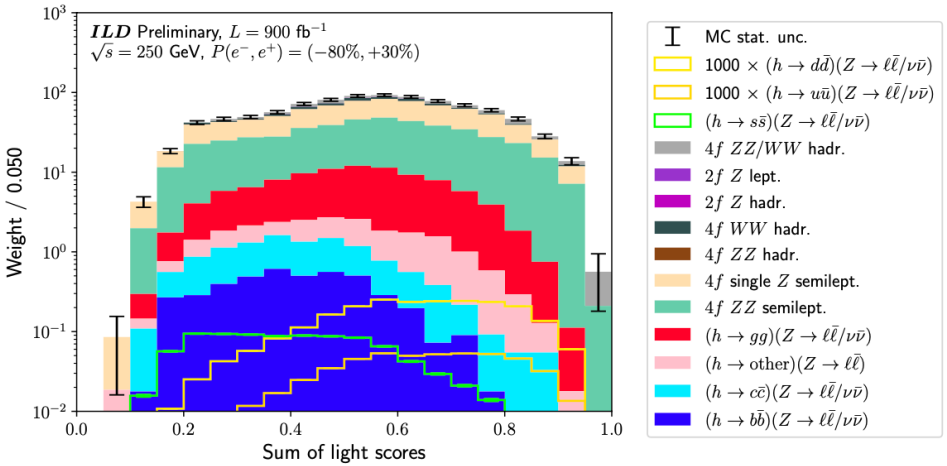

(b) $Z \to \ell\bar{\ell}$ channel

Figure D1: Fit discriminants for each channel of the SM $h \to d\bar{d}$ and $h \to u\bar{u}$ analyses, Eq. D3. Each histogram is produced at the level of the last selection of their respective channel in Table 3. The error bars represent the MC statistical uncertainties. The sum-of-weights per process is normalised to the SM cross section. N.B. the $h \to s\bar{s}$, $h \to d\bar{d}$, and $h \to u\bar{u}$ signals are unstacked, with the latter two scaled by a factor of 1,000.

u/d Yukawa couplings

2203.07535

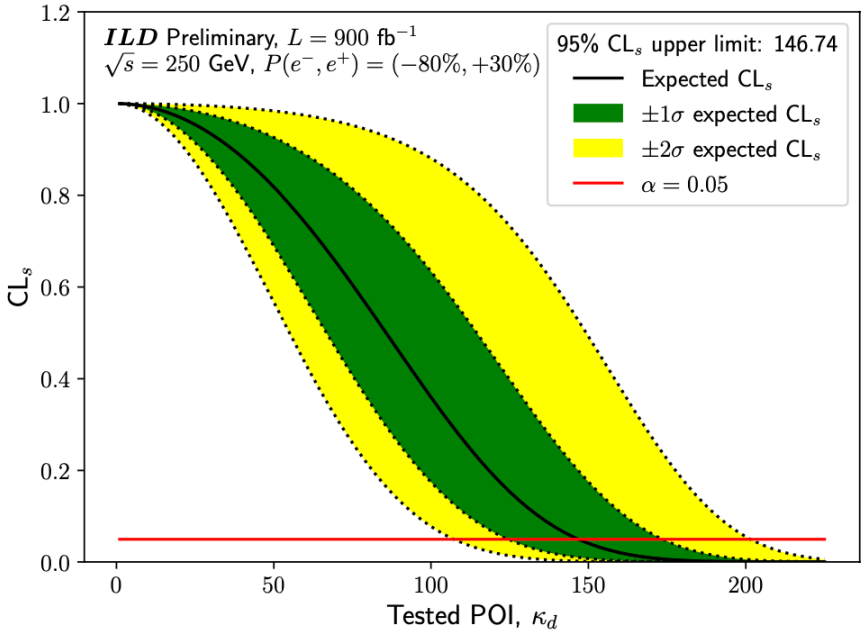

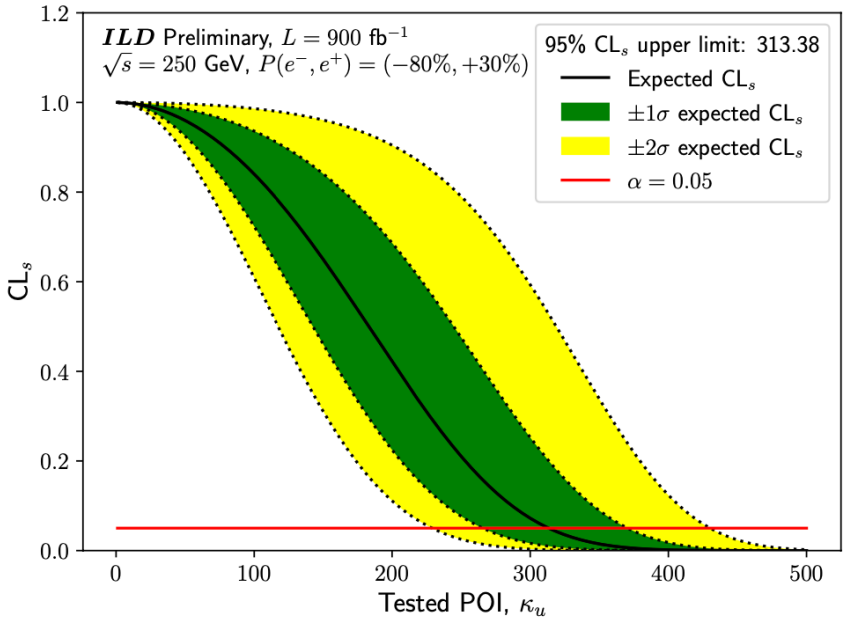

d-Yukawa couplings

2203.07535

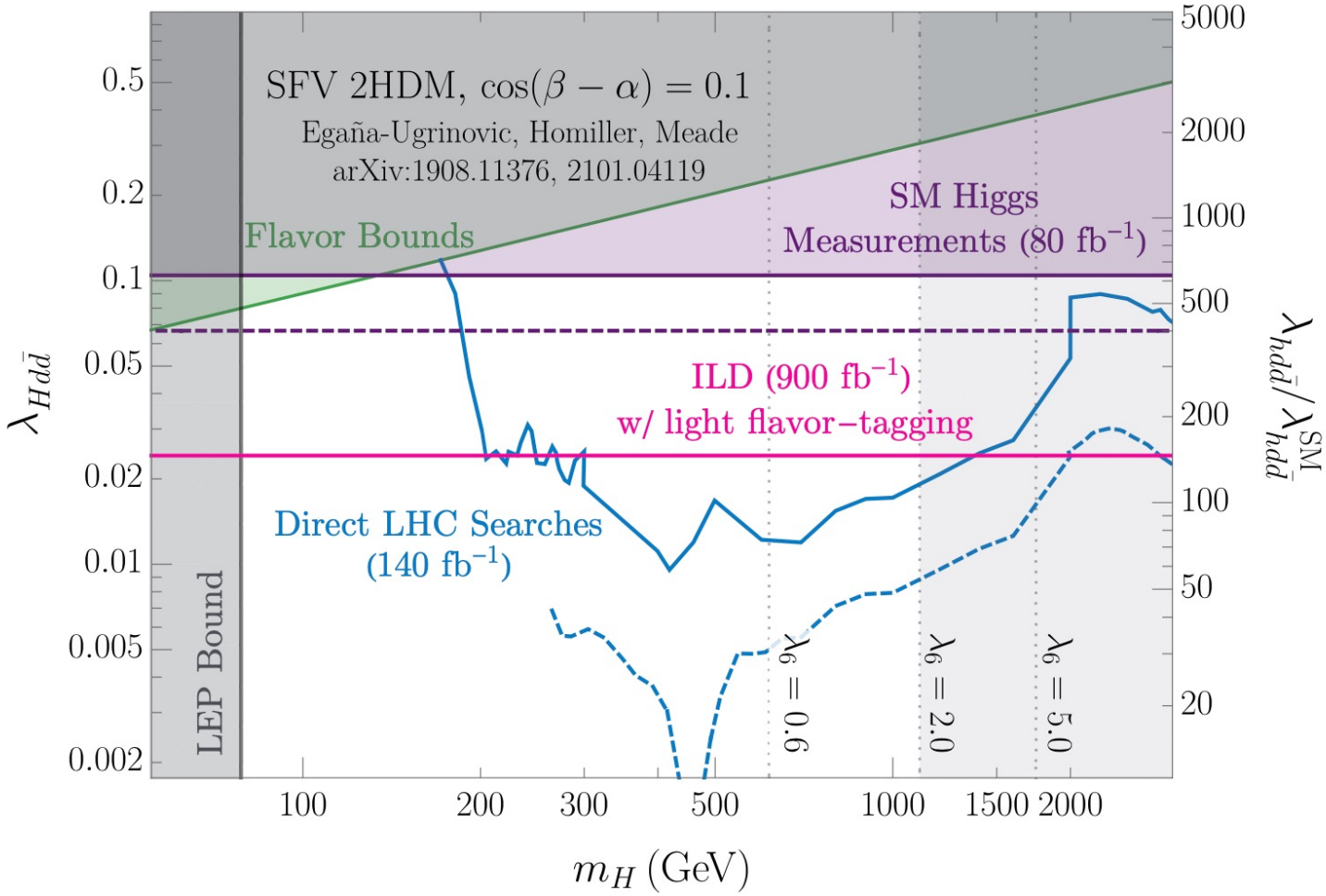

Figure D3: 95% CL bounds on the CP-even Higgs-down Yukawa coupling $\lambda_{Hd\bar{d}}$ as well as on 125 GeV SM Higgs-down Yukawa coupling $\lambda_{hd\bar{d}}/\lambda^{\rm SM}_{hd\bar{d}}$ (i.e., κ_d) for the SFV 2HDM described in Refs. [23, 24]. The pink line shows the bounds obtained from the $h \to d\bar{d}$ analysis presented in this appendix. See the caption of Fig. 23 for further details.

Gaseous RICH with SiPMTs

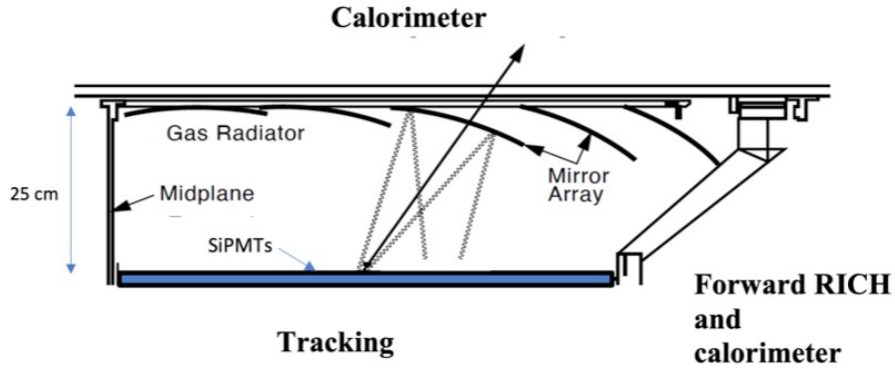

(a) Side view of overall layout

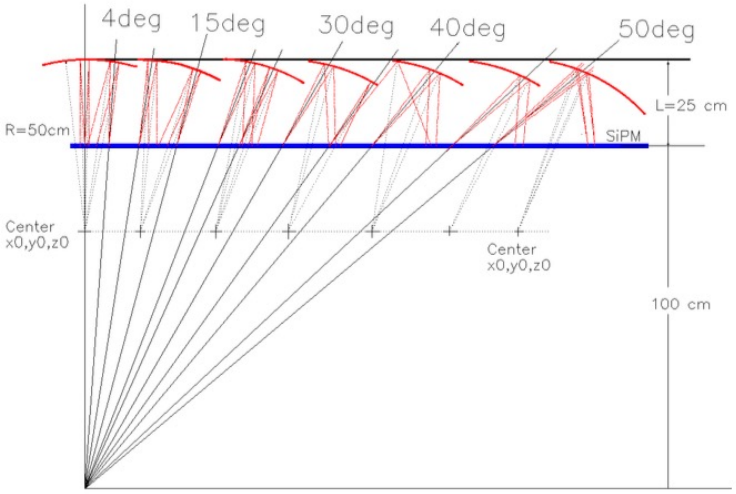

(b) Side view with tracks

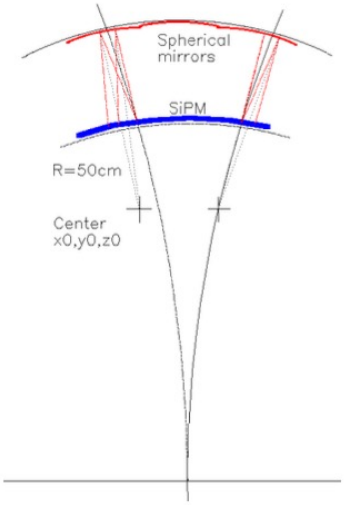

(c) Front view with tracks

Figure 24: Proposed gaseous RICH detector at SiD/ILD. (a) The relative placement of the tracking, calorimetry, and forward instrumentation is indicated. (b) Side view and (c) front view of the proposed detector, with tracks. All of the mirrors have a radius of 50 cm. This optical design is preliminary as further tuning of the mirror positions is required.

Gaseous RICH with SiPMTs – gas

- **Low mass vessel** (total detector weight is small compared to CRID @ SLC - no liquid radiator, no heavy mirrors, etc)

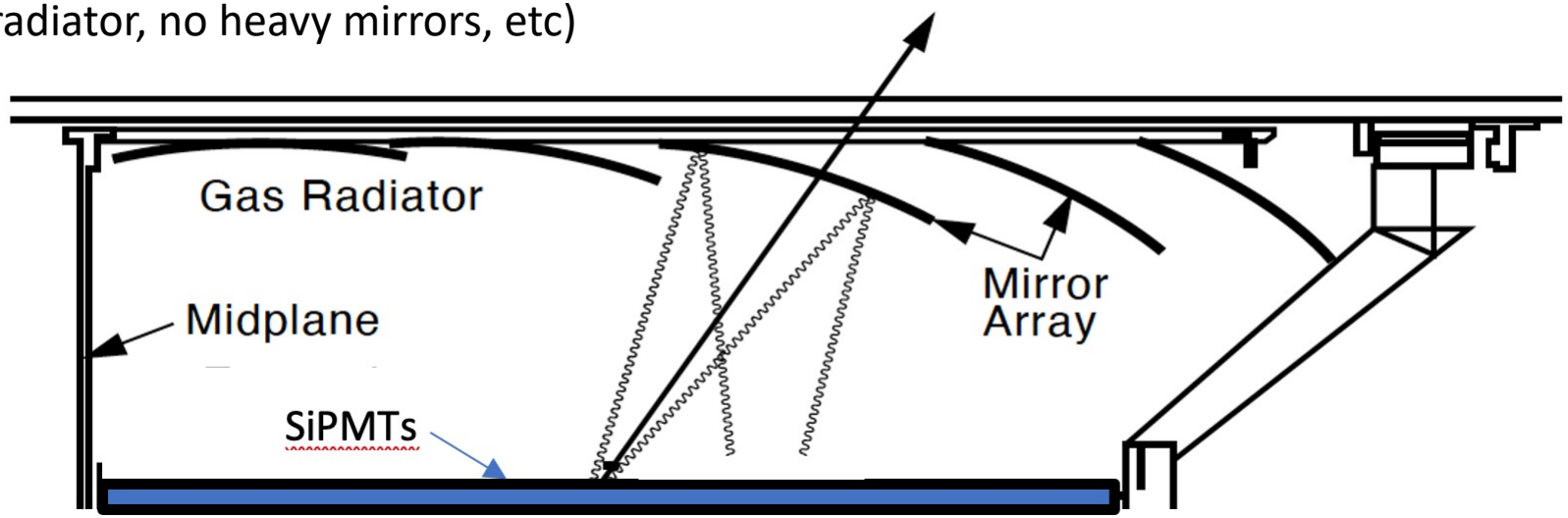

6.1.1 Gas choices

(a) Pure C_5F_{12} gas at 1 bar requires a detector temperature of 40 °C since the boiling point of this gas is 31 °C at 1 bar. That could prove to be difficult since SiPMs need to be cooled.

(b) A gas choice of pure C_4F_{10} at 1 bar allows detector operation at a few degrees Celsius since boiling point of this gas is -1.9 °C at 1 bar. This is presently our *preferred* choice.

(c) A choice of C_2F_6 gas at 1 bar would allow detector operation even below 0 °C since the boiling point of this gas is -70.2 °C at 1 bar. However, this gas would deliver insufficient number of photoelectrons in the geometry shown in Fig. 24 and therefore it was not considered.

(d) A choice of C_3F_8 gas at 1 bar would allow detector operation at -30 °C since the boiling point of C_3F_8 is -37 °C. The detector's PID performance will be between C_2F_6 and C_4F_{10}. It is certainly worthwhile to look into this solution.

(e) Among non-freon-based gases, one could consider either C_3H_8 or C_3H_6, each of which has a reasonably high refraction index; however, these gases are flammable.

Gaseous RICH with SiPMTs – refraction index, mirror reflectivity, PDE

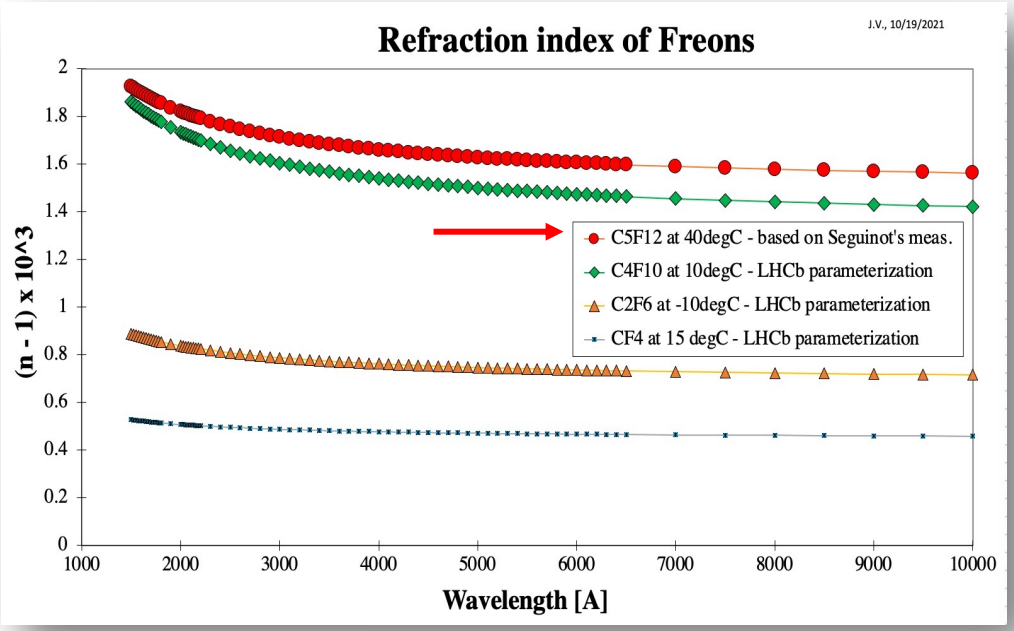

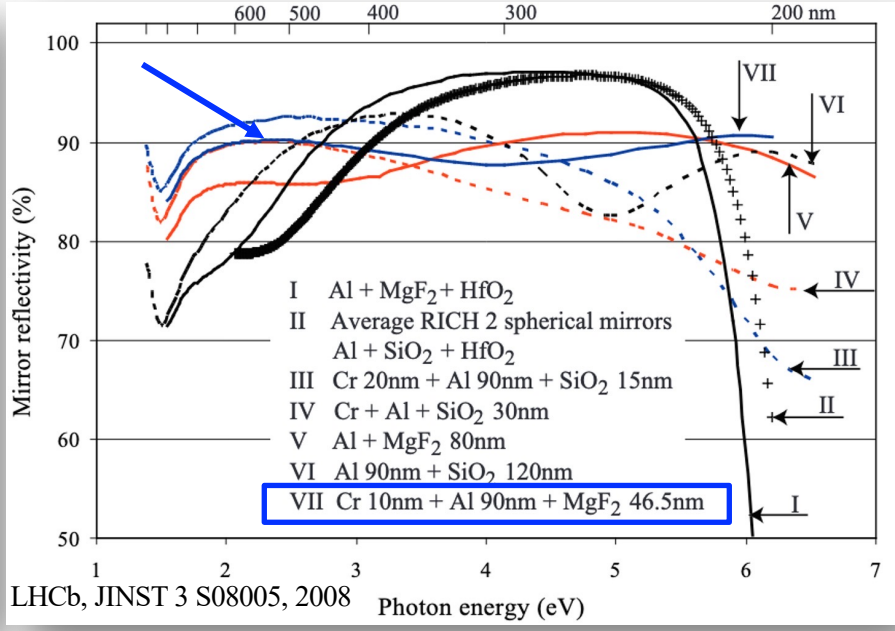

LHCb, JINST 3 S08005, 2008

P. Krizan et al.,NIMA 990(2020)163804, and R. Klanner, arXiv:1809.04346v2, 2018

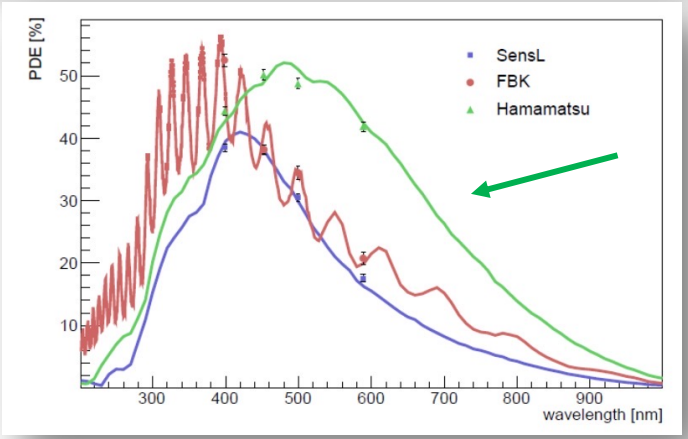

PDE = Photon detection efficiency:

$$PDE = FF \times QE(\lambda) \times P_T(V_{bias}, \lambda)$$

QE(λ) – QE of Si
FF – Fill factor within one SiPMT
$P_T(V_{bias}, \lambda)$ – Trigger efficiency

In addition, a SiPMT array has losses due to gaps between pixel elements.
Jerry used **65%** in his calculations, could jump to 100% with back-illumination.

Gaseous RICH with SiPMTs – performance

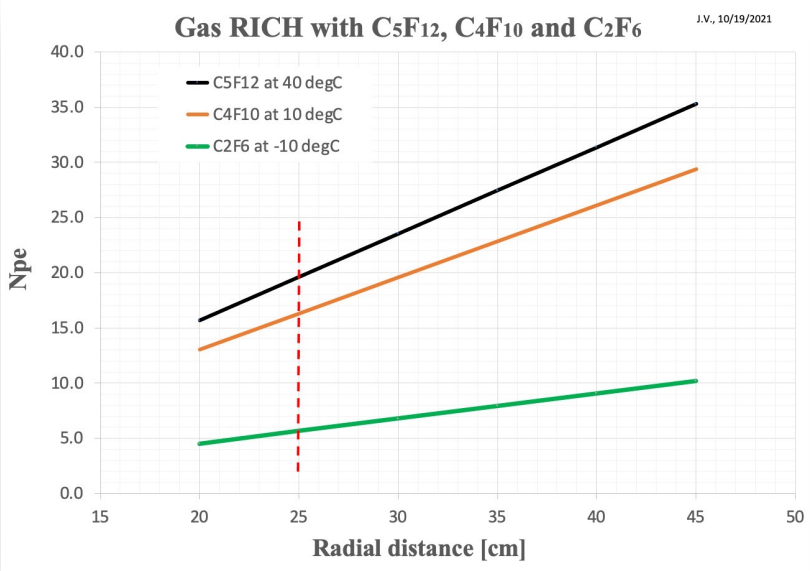

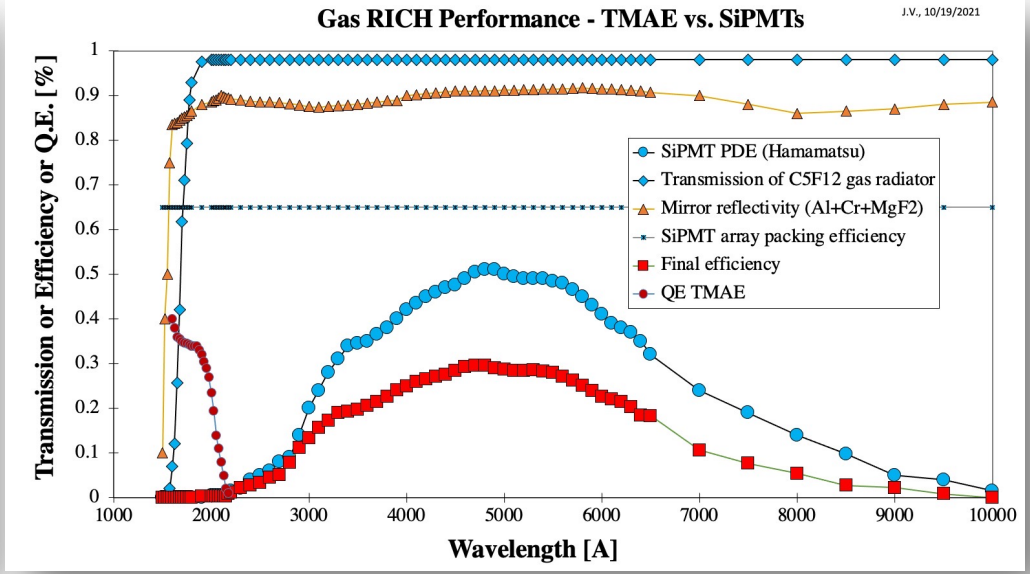

C_4F_{10} seems a possible solution with SiPMT readout even for 20-25 cm radial distance!

Much better Cherenkov Photon Detection efficiency over a wider wavelength compared to TMAE

Why didn't we do this before?
No SiPMT!

Gaseous RICH with SiPMTs – performance

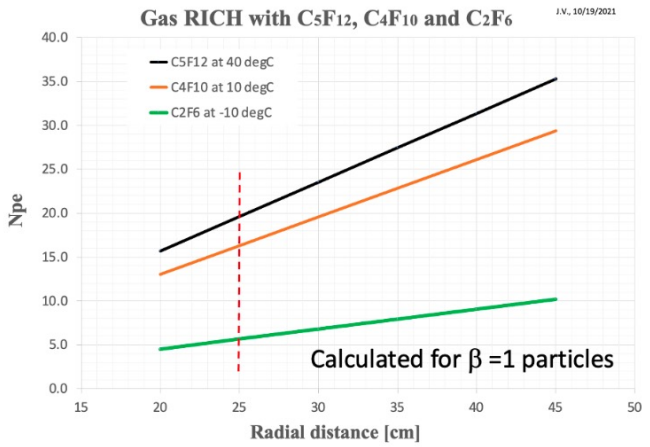

(a)

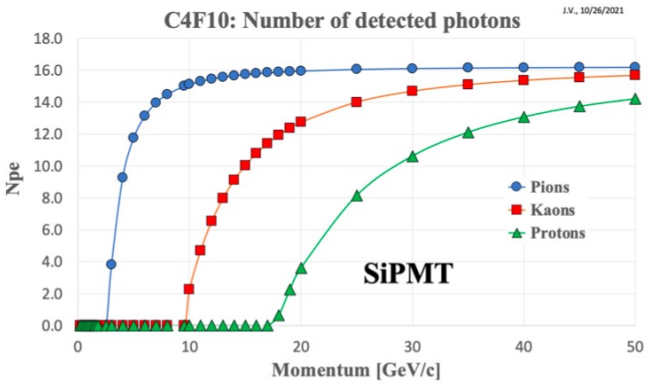

(b)

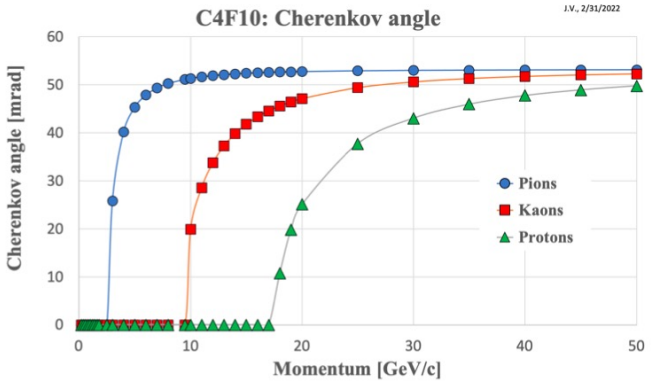

(c)

Figure 23: (a) Calculated number of photoelectrons per ring as a function of radiator length L. (b) Calculated number of photoelectrons and (c) Cherenkov angle as a function of momentum for pions, kaons, and protons. One can see that the kaon threshold is ~10 GeV for C_4F_{10} gas and the expected number of photoelectrons per ring is about 16 for $L = 25$ cm and $\beta \sim 1$.

Gaseous RICH with SiPMTs – performance

- Track bending effects are sizable and depend on the magnetic field
- Photon can be produced anywhere along the track segment along path L, which smears the Cherenkov angle
- Bending effects have been evaluated for various $\theta_{dip} = 90°, 86°, 70°$

Jerry's sketches

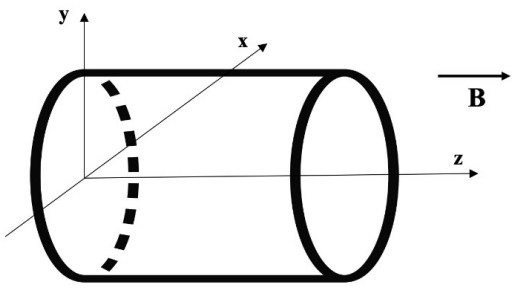

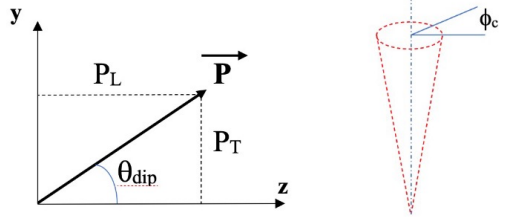

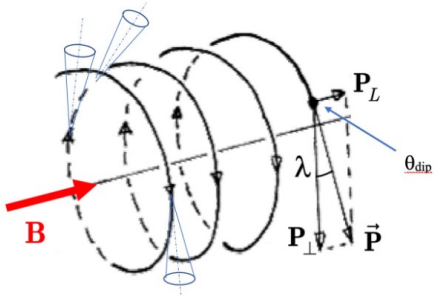

- **Cherenkov cone rotates in 3D !**

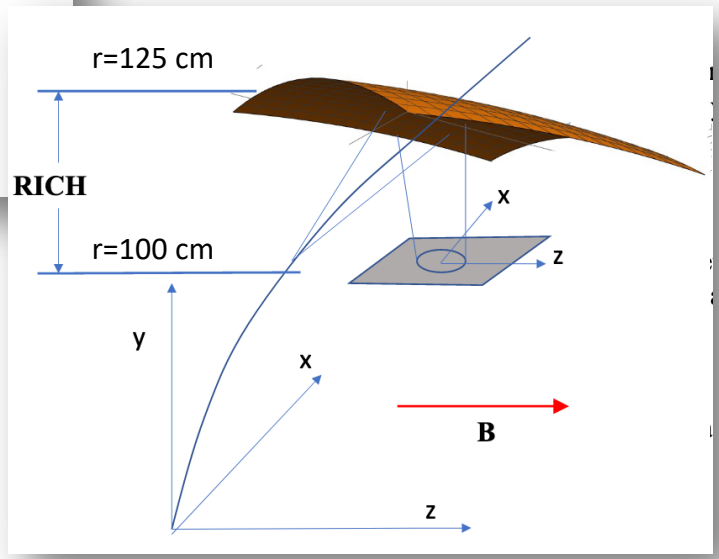

Gaseous RICH with SiPMTs – performance

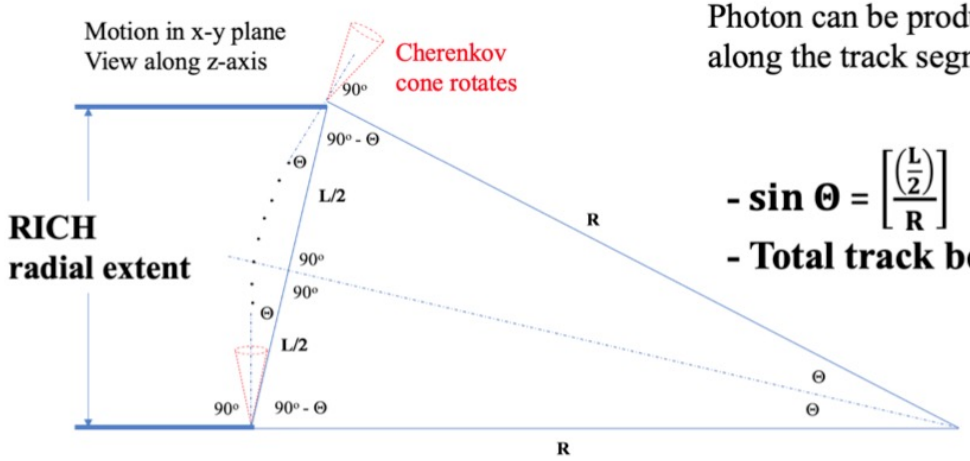

Photon can be produced anywhere along the track segment along path L

- $\sin\Theta = \left[\frac{\left(\frac{L}{2}\right)}{R}\right]$
- Total track bend angle: 2Θ

$$\sigma_{\theta c} \sim \frac{2\,\Theta}{\sqrt{12}} \sim \{2\,\arcsin\left[\frac{\left(\frac{L}{2}\right)}{R}\right]\}\frac{1}{\sqrt{12}}\ , R = \frac{p}{300\,B}, L = 0.25\ \text{m}, p\ [\text{MeV/c}], R\ [\text{m}]$$

(a)

L = 15 cm

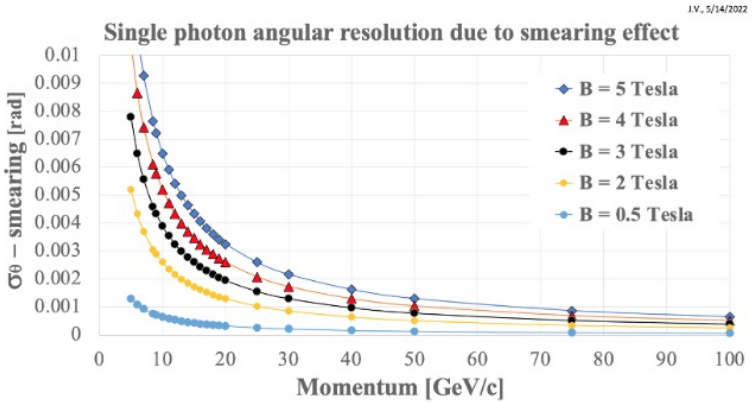

L = 25 cm

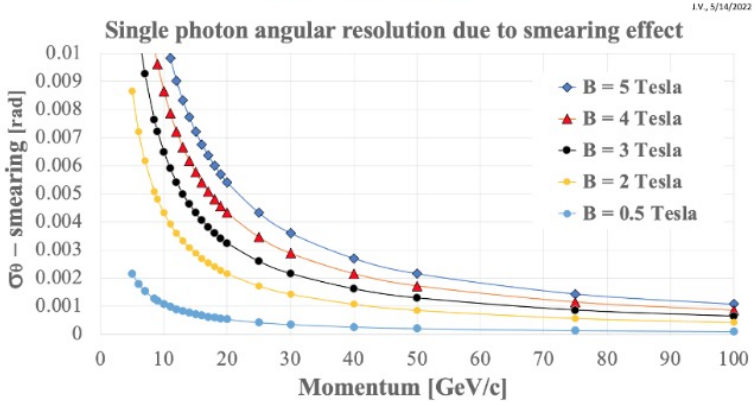

Gaseous RICH with SiPMTs – performance

$\sigma_\theta = s_{\text{single photon}}/\sqrt{Npe} \otimes \sigma_{\text{tracking}} = \sqrt{\{\sigma_{\text{chromatic}}^2 + \sigma_{\text{pixel}}^2 + \sigma_{\text{smearing effect}}^2\}}/\sqrt{Npe} \otimes \sigma_{\text{tracking}}$

σ_{smearing} = **analytical formula** , $\sigma_{\text{chromatic}} \sim$ **0.85 mrad**, **pixel size: 3 mm**, $\sigma_{\text{tracking}} \sim$ **0.5 mrad**, **L = 25cm, 1 bar**

S [# of sigma]

$$= \frac{\theta_\pi - \theta_K}{\sigma_\theta}$$

σ_θ is total photon angle resolution, which includes:

$\sigma_{\text{single photon}}/\sqrt{Npe} \otimes \sigma_{\text{tracking}}$

$Npe = (N_{\text{Pion}} + N_{\text{Kaon}})/2$

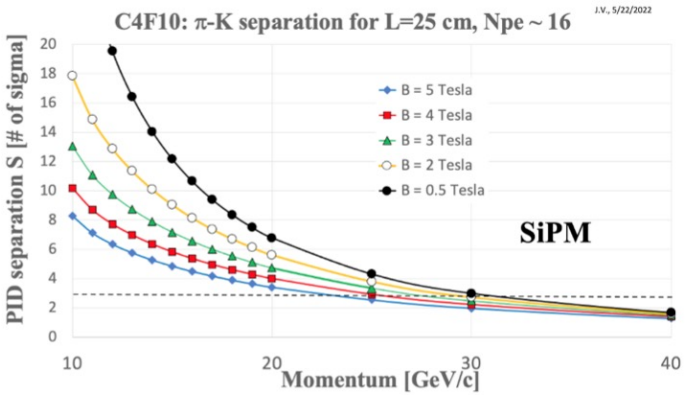

(a) Nominal design

$\sigma_\theta = \sigma_{\text{single photon}}/\sqrt{Npe} \otimes \sigma_{\text{tracking}} = \sqrt{\{\sigma_{\text{chromatic}}^2 + \sigma_{\text{pixel}}^2 + \sigma_{\text{smearing effect}}^2\}}/\sqrt{Npe} \otimes \sigma_{\text{tracking}}$

σ_{smearing} = **analytical formula** , $\sigma_{\text{chromatic}} \sim$ **0.85 mrad**, **pixel size: 0.5 mm**, $\sigma_{\text{tracking}} \sim$ **0.3 mrad**, **increase PDE by 20%**

S [# of sigma]

$$= \frac{\theta_\pi - \theta_K}{\sigma_\theta}$$

σ_θ is total photon angle resolution, which includes:

$\sigma_{\text{single photon}}/\sqrt{Npe} \otimes \sigma_{\text{tracking}}$

$Npe = (N_{\text{Pion}} + N_{\text{Kaon}})/2$

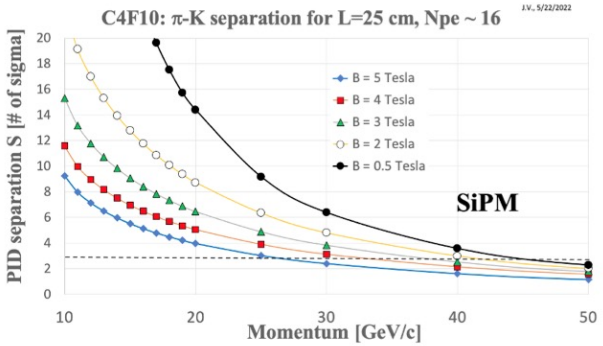

(b) Design with improved performance

PID Performance of the Compact RICH with SiPMTs

- Smearing effects increase with magnetic field and dip angles while decrease with momenta.
  - The contribution of various effects has been estimated, see much more in the back-up slides

Table 4: Various contributions to the Cherenkov angle resolution.

Single-photon error source	SiD/ILD RICH detector @ 5 T [mrad]	SLD CRID detector @ 0.5 T [mrad]
Chromatic error	~0.85	~0.4
Pixel size error ($0.5\times0.5 - 3\times3\,mm^2$)	0.4–2.3	~0.5
Smearing effect due to magnetic field	1.5–2.5	~0.5
Mirror alignment	$\ll 1$	~1 (?)
Other systematic errors	$\ll 1$	a few mrad
Total single-photon error	1.8–3.5	~3.4
Total error including systematic effects	–	~4.3
Tracking angular error	~0.5	~0.8 [93, 94]

These results justify a full Geant 4 simulation!

ARC vs Compact RICH

ARC	Compact RICH
C4F10 at 3.5 bar	C4F10 at 1 bar
~10% X0	~4-5% X0
SIMPTs at -30 (C4F10 condenses at +2degC. Aerogel on top of SiPMT will act as an insulation/radiator.)	SIMPTS at room temperature
Gaps between active SiPMT sensor segments	continuous coverage with only small gaps between SiPMT sensors (similar to CRID)
chromatic error ~0.5 mrad (possibly having Aerogel helps as it is acting as a UV filter, thus removing part of the wavelength acceptance and therefore reducing chromatic error.)	chromatic error ~0.9 mrad
tracking resolution ~**0.3 mrad**	tracking resolution ~**0.8 mrad** based on SLD experience
1 mrad for angular resolution thanks to **0.5mm^2 pixels**	error from final size pixels **~0.8-2.3 mrad** if we use **1mm^2 or 3mm^2** pixel sizes
No smearing due to magnetic field (2 T)	~1.5-2.5 mrad smearing due to magnetic field (5 T)
25 photoelectrons for 20 cm (higher QE using NUV-HD SiPMTs)	16 photoelectrons per ring at beta = 1 and 25 cm radiator length
SIMPTs with **10 ps** timing resolution	SIMPTs with **~100 ps** timing resolution